A method for Se isotope analysis of low ng-level geological samples via double spike and hydride generation MC-ICP-MS

Timon Kurzawa[a,*], Stephan König [a], Jabrane Labidi [a], Aierken Yierpan [a] and Ronny Schoenberg [a]

[a]Isotope Geochemistry, Department of Geosciences, Eberhard Karls Universität Tübingen, Wilhelmstraße 56, 72074 Tübingen. Germany

*Corresponding author (phone: +49 7071 29-74991; e-mail: timon.kurzawa@uni-tuebingen.de)

Abstract

The isotopic signature of the chalcophile, redox-sensitive and moderately volatile element Se in geological materials may offer valuable new insights into the origin and evolution of volatiles in planetary systems. Here, we report a new method for Se isotope determination of low Se containing samples relevant to the Earth's mantle reservoir. We present a method that combines a double spike and hydride generation sample introduction system with a ThermoFisher Scientific® Neptune*Plus*™ MC-ICP-MS. The measurement routine takes advantage of methane injection in the instrument source during measurement, resulting in enhanced Se signals and suppression of polyatomic interferences. Purification of Se from natural samples was simplified by employing conventional ion exchange chromatography procedures. An external reproducibility of 0.15 ‰ (2σ) on $\delta^{82/76}$Se values for measurements performed on natural samples with Se abundances down to ~ 5 ng is obtained. We demonstrate that our technique allows the determination of Se isotope signatures of low Se-bearing geological materials with complex matrices such as mafic igneous rocks, which is essential to extend the Se isotopic investigation to Se-depleted planetary reservoirs such as the Earth's mantle.

Keywords

Selenium isotopes, heavy stable isotopes, double spike hydride generation MC-ICP-MS, mantle geochemistry

1 Introduction

Selenium (Se) is a redox-sensitive element with the valence states -II, 0, +VI, +VI and a total of six stable isotopes (^{74}Se, ^{76}Se, ^{77}Se, ^{78}Se, ^{80}Se and ^{82}Se). The potential for Se isotopes to study low-temperature redox processes on the Earth's surface has been shown in various studies (Clark and Johnson, 2010; Ellis et al., 2003; Johnson and Bullen, 2003; Johnson and Bullen, 2004; Johnson et al., 2000; Johnson et al., 1999; Mitchell et al., 2013; Rouxel et al., 2004; Rouxel et al., 2002; Schilling et al., 2014; Schilling et al., 2011; Schilling et al., 2013; Shore, 2011; Wen and Carignan, 2011; Zhu et al., 2014). In addition, Earth's atmospheric redox evolution has more recently been studied by examining the redox state of the oceans using Se isotopes in the ancient sedimentary record (e.g. Kipp et al., 2017; Mitchell et al., 2016; Pogge von Strandmann et al., 2015; Stüeken et al., 2015a; Wen et al., 2014, and references therein). Moreover, Se isotope systematics have been evaluated as a possible tracer for the volatile evolution of meteoritic material and planetary reservoirs (Vollstaedt et al., 2016a; Vollstaedt et al., 2016b). To this end low Se containing planetary reservoirs such as the Earth's mantle need to be more firmly constrained and require new Se isotopic data which need to be placed in context of its elemental behavior.

In the Earth's mantle, Se is an ultra-trace element, with typical Se content < 100 ng g^{-1} in lherzolites (Lorand and Alard, 2010). Although small fractions of Se can be present in silicates (Tamari et al., 1990), Se mostly is concentrated in micrometric sulfides and is accordingly considered chalcophile (Hattori et al., 2002; König et al., 2014; Lorand et al., 2013; Luguet et al., 2004). In contrast to the highly siderophile elements (HSE, Os, Ir, Ru, Rh, Pt, Pd, Re, Au), studies involving Se in mantle-derived rocks are still relatively rare (Alard et al., 2011; Lorand and Alard, 2010; Lorand et al., 2003; Lorand et al., 2004; Morgan, 1986), although more recent high-precision isotope dilution studies on Se in fertile and depleted peridotites and pyroxenites have emerged (König et al., 2015a; König et al., 2014; König et al., 2012; Wang and Becker, 2013; Wang et al., 2013). These are complemented by geochemical and experimental studies on Se behavior during mantle melting (Brenan, 2015; Lissner et al., 2014; Marchesi et al., 2013).

The Se concentration in the Earth's mantle is estimated to be ~ 80 ng g^{-1} (McDonough and Sun, 1995; Wang and Becker, 2013). When normalized to a CI chondrite, the Se depletion degree is

~ 0.0037 x CI (Palme and O'Neill, 2003; Vollstaedt et al., 2016a), similar to but somewhat lower than what is observed for the HSEs (Becker et al., 2006). These elements altogether show a roughly chondritic pattern and an excess abundance in the Earth's mantle compared to those predicted following core-mantle differentiation (Lorand et al., 2008; Morgan et al., 2001; Walker, 2009). This is widely explained by late accretion of chondritic material (e.g. Kimura et al., 1974; Mann et al., 2012; Walker, 2009) shortly after core-mantle differentiation.

Due to its volatile character, Se links late accretion with the origin of other volatiles such as e.g. S, Te, Zn but also highly volatiles components like H_2O, C, or N_2 (McDonough and Sun, 1995; Wang and Becker, 2013). Understanding the origin and evolution of Se in the Earth's mantle-crust-atmosphere system may thus help to constrain the origin of volatile components on Earth. However, it remains controversial whether the Se systematics in mantle rocks allow description of late accreted components (Wang and Becker, 2013), or metasomatic processes in the mantle (König et al., 2014; König et al., 2015b; Wang and Becker, 2015). A new perspective provided by the isotopic signature of Se may help in this context. Yet analyses remain challenging because igneous rocks contain orders of magnitudes lower Se concentrations in the range of 10 to 200 ng g^{-1} (König et al., 2014; Lissner et al., 2014) compared to sediments with μg g^{-1} levels of Se. Hence, an analytical technique is needed to precisely and accurately determine the Se isotope ratio of low abundance geological materials including igneous rocks such as basalts. Here we present a method for Se isotope measurements of such samples with Se concentrations of few tens of nanograms, using a double spike technique and a hydride generation introduction system on a Neptune*Plus*™ MC-ICP-MS.

2 Materials and analytical techniques

2.1 Reagents and materials

All sample digestions, chemical purifications and instrumental measurements were performed at the ISO-5 (US FED standards class 100) clean-room facilities of the Isotope Geochemistry Group at the University of Tübingen, Germany. De-ionized water was further purified with a Merck Millipore Milli-Q™ system to 18.2 MΩ × cm at 25 °C. All acids used during digestion, sample preparation and measurements were distilled from MERCK Millipore Emsure™ grade HNO_3 (65 %) and HCl (37 %)

with Savillex™ DST-1000 Acid Purification Systems and diluted to required molarities to ± 0.03 mol L^{-1} as checked by titration. Eichrom™ ion exchange resins, beakers, vials for centrifugation and analysis were pre-cleaned with multi-step HCl-HNO_3 treatments.

Two Se standard solutions with different Se isotopic compositions were used. The Se standard reference material SRM-3149 (Lot.-#: 100901; 10.042 ± 0.051 mg-g^{-1}) was purchased from the National Institute of Standards and Technology (NIST). NIST SRM-3149 is now widely used as δ-zero reference material for Se isotope measurements (Carignan and Wen, 2007). The second standard solution used in our study is MH-495, previously used as an in-house Se solution at the University of Urbana, Illinois and generously provided by T. M. Johnson (Johnson and Bullen, 2004; Johnson et al., 1999). This standard solution was created from reagent-grade Se^0 pellets at the University of California at Davis by Mitchell Herbel (Johnson et al., 1999) and shows a $\delta^{82/76}$Se isotope ratio lower than the reference value for NIST SRM-3149 by -3.04 ± 0.50 ‰ (2σ, n = 2) (Carignan and Wen, 2007) to - 3.44 ± 0.06 ‰ (2σ, n = 5) (Zhu et al., 2014).

For comparison to previously published Se isotope results we chose the two US Geological Survey (USGS) shale reference materials SGR-1 and SCo-1 (e.g. Pogge von Strandmann et al., 2014; Rouxel et al., 2002). These shales have relatively high Se concentrations (SGR-1: 3.50 ± 0.28 μg g^{-1}; SCo-1: 0.89 ± 0.06 μg g^{-1}) (Gladney and Roelandts, 1988) and comparison to other studies is possible (Kipp et al., 2017; Mitchell et al., 2012; Pogge von Strandmann et al., 2014; Rouxel et al., 2002; Schilling et al., 2011; Stüeken et al., 2013; Stüeken et al., 2015b; Stüeken et al., 2015c; Vollstaedt et al., 2016a). We also selected the USGS BCR-2 (~77.8 ± 6.4 ng g^{-1}, 2σ, n = 5) (Lissner et al., 2014), which has a factor 50 lower Se concentration compared to the USGS shales, can be compared to data reported by Rouxel et al. (2002) and is suitable as a geological reference to terrestrials basalts.

2.2 Sample digestion and Se purification

Between 10 to 1000 mg of sample powder were weighted into quartz glass vessels (15, 50 or 90 ml) and mixed with an adequate amount of the ^{77}Se-^{74}Se double spike solution. We report accuracy tests where variable amount of in-house standard solution MH-495 was additionally admixed to some samples (section 3.2). Depending on the sample weight 2.5 to 7.5 ml inverse aqua regia (3:1 molar ratio; conc.

109 HNO_3 : conc. HCl) were added, the vessels were subsequently sealed with Teflon-tape and placed in a
110 high-pressure asher (HPA-S, Anton Paar™). During digestion for 16 hours at 220 °C and 100 bar, Se
111 was extracted from the sample material and equilibrated with the Se double-spike.

112 Several studies emphasize Se loss in the presence of HCl while evaporating at temperatures
113 exceeding 80 to 85 °C (Layton-Matthews et al., 2006; Pogge von Strandmann et al., 2014; Rouxel et al.,
114 2002; Stüeken et al., 2013; Wang et al., 2013). This is because of the formation of volatile Se-species
115 (e.g. Stüeken et al., 2013; Vollstaedt et al., 2016a). Special care was taken during subsequent chemical
116 purification: Se solutions were dried down without exceeding 65 °C and re-dissolved in concentrated
117 HCl to convert all Se^{6+} to Se^{4+} (Elwaer and Hintelmann, 2008; Pogge von Strandmann et al., 2014).

118 Previous studies have demonstrated that the purification of Se from a sample matrix can be
119 challenging in terms of quantitative recoveries from ion exchange resins and a potentially associated
120 mass-dependent fractionation (e.g. Pogge von Strandmann et al., 2014). Thiol cotton fibre (TCF) or
121 powder (TCP) is one way to separate Se from its sample matrix. This method allows recovering ≥ 98 %
122 of the initial Se (Elwaer and Hintelmann, 2008; Rouxel et al., 2002) and has been used for routine
123 determination of Se concentrations of rock reference materials at low ng levels (e.g. König et al., 2012;
124 Marin et al., 2001; Yu et al., 1983). The relatively high Se yield and the additional advantage of a
125 simultaneous Te purification is considered a good choice for concentration analysis (Yu et al., 1983).
126 The use of TCF/TCP can lead to the formation of insoluble salts and organic-derived interferences on
127 Se masses (Pogge von Strandmann et al., 2014). Thus, TCF-/TCP-handled samples require careful
128 treatment with HNO_3 and H_2O_2 (König et al., 2012; Pogge von Strandmann et al., 2014; Rouxel et al.,
129 2002). In order to test the instrumental capabilities we here describe a simpler technique adapted from
130 Fehr et al. (2004) and Wang et al. (2013). This involves the combination of conventional ion exchange
131 chromatography procedures with hydride generation. The following procedure has been optimized for
132 Se purification and yields.

133 First, the dried samples obtained after a first evaporation were dissolved with 4 mL 6 mol L^{-1}
134 HCl and centrifuged at 5000 rpm for 10 min. Before loading the sample solutions onto Spectra/Chrom®
135 Disposable MiniColumns containing 3 mL of Eichrom® AG1-X8 anion resin (100-200 mesh), the resin
136 was washed with 3 ml of 1 mol L^{-1} HNO_3 twice and conditioned with 2x 3 ml 6 mol L^{-1} HCl. While Fe

was retained as $FeCl_4^-$ by the resin, Se was not adsorbed but collected together with other matrix elements in 12 mL 6 mol L^{-1} HCl. The collected Se-containing solutions were evaporated to dryness at $T \leq 65$ °C. The dried down solutions were then taken up in 4 ml 0.06 mol L^{-1} HNO_3 for purification by cation exchange chromatography using Spectra/Chrom® Disposable MiniColumns containing 3 ml of Eichrom® AG50W-X8 resin (100-200 mesh) (e.g. Wang et al., 2013). The cation exchange resin was washed with 6 mol L^{-1} HCl and H_2O and conditioned with 6 mL 0.06 mol L^{-1} HNO_3 before loading the samples. Se was collected in 12 mL 0.06 mol L^{-1} HNO_3 while other matrix elements were retained on the resin under these conditions. The solutions containing Se were again dried at $T \leq 65$ °C on a hotplate, re-dissolved in 2 mol L^{-1} HCl and heated in closed beakers on a hotplate at 80 °C for several hours to achieve complete reduction of Se^{6+} to Se^{4+} (Elwaer and Hintelmann, 2008; Pogge von Strandmann et al., 2014). Typically our total procedural blanks remain below detection limit and only in some cases show up to 1 ng, likely mirroring randomly suboptimal HPA-S glass vial treatment. While this still represents only < 1 % of bulk Se for most samples analyzed here, multiple replicate digestions of all samples were performed in order to verify results with different blank levels including for lower Se containing samples. Although blanks are generally too low to determine an isotopic composition, high reproducibility for various blank levels confirms that blanks are negligible.

2.3 The role of the double spike

Metallic selenium enriched in ^{77}Se and ^{74}Se tracer material in metal form was obtained from ISOFLEX. Upon dissolution in 2 mol L^{-1} HNO_3, a double spike solution with a composition of ~ 52 % ^{74}Se and ~ 47 % ^{77}Se was prepared taking the error propagation calculations after Rudge et al. (2009) into account. After dilution, the normality of nitric acid in the double-spike solution was 0.1 mol L^{-1}. Other Se isotopes account for < 1 % of the double spike solution as shown in Table 1, which also gives a comparison to double spike compositions used in other studies. Provided that sample and spike are well equilibrated prior to chemical purification, double spike methods have already been demonstrated to be suitable for Se stable isotope analyses (Clark and Johnson, 2010; Johnson et al., 1999; Pogge von Strandmann et al., 2014; Vollstaedt et al., 2016a; Zhu et al., 2008).

[TABLE 1]

The spike was calibrated against the NIST SRM-3149 Se solution. Various proportions of spike-sample ratios (f_{spike} from 0.1 to 0.9, n = 9) were tested. To increase the small volumes of NIST SRM-3149 and double spike, an additional 2 mL of 2 mol L^{-1} were added. To achieve equilibration the mixtures were heated at 80 °C in a closed beaker for a minimum of 2 h. The mixtures were then dried down at 65 °C and re-dissolved in 2 mol L^{-1} HCl, again heated at 80 °C for 2 h to ensure that all Se is reduced and finally measured. All measured mixtures of f_{spike} varying from 0.1 to 0.8 give $\delta^{82/76}$Se within our long-term reproducibility for NIST SRM-3149 of 0.00 ± 0.11 ‰ (2σ, n = 350) (filled circles in Fig. 1a). Note that the mixture with the lowest f_{spike} = 0.1 has a significantly larger internal uncertainty (2 s.e error bars in Fig. 1a) and the mixture with the highest f_{spike} = 0.9 is outside of the external reproducibility of 0.11 ‰ given by all other mixtures with f_{spike} between 0.2 and 0.8. This provides a lower and upper limit of acceptable double spike-sample ratios. Within the wide range of f_{spike} between 0.2 and 0.8 the ^{74}Se-^{77}Se double spike used in this study thus allows for accurate Se isotope measurements. A systematic shift to heavier $\delta^{82/76}$Se of 0.18 ± 0.10 ‰ (2σ, n = 7) is observed for mixtures that were not allowed to equilibrate as described above (open circles in Fig. 1a), but directly dried down after mixing. This may be due to preferential loss of light Se isotopes during evaporation, even at temperatures below 65 °C, prior to full equilibration of standard and spike Se and emphasizes that careful treatment is crucial.

[FIGURE 1]

Based on the above observation, we further tested the possibility of Se isotope fractionation during partial Se loss by evaporation from solutions with HCl. For this, NIST SRM-3149 solutions were dried down at 65 °C without spike addition. The Se isotope measurements were then performed with two different analytical approaches, one involving the sample-standard bracketing (SSB) (Stüeken et al., 2013) and the other the double spike measuring method (e.g. Pogge von Strandmann et al., 2014; Vollstaedt et al., 2016a). For the SSB approach a 50 ng mL^{-1} NIST SRM-3149 Se solution was used as the bracketing standard, yielding ^{82}Se voltages of roughly 1.5 V (using an amplifier resistor of 10^{11} Ω). Sample solutions were then prepared to match the signal intensity of the standard within 10 % intensity. Samples and standards were measured for 100 cycles each having an integration time of 4.194 s. Over the measurement session, Se in-house solution (MH-495) was measured versus the NIST SRM-3149

standard solution. These solutions were taken directly out the main batch and were not dried. SSB measurements yielded average $\delta^{82/76}$Se of -3.25 ± 0.03 ‰ (2σ, n = 4), indistinguishable from our double-spike value (MH-495: -3.27 ± 0.13 ‰, 2σ, n = 100) (see section 3.1). For the SSB approach, four solutions were processed and Se losses varying between 5 and 30 % yielded $\delta^{82/76}$Se values ranging between 0.43 ± 0.31 ‰ and 1.85 ± 0.31 ‰ (Fig. 1b, open circles). For the double spike measuring approach, five NIST SRM-3149 solutions were doped with an adequate amount of the double spike after evaporation and prior to mass spectrometric determinations, which were performed on ~ 15 ng mL^{-1} Se solutions. Evaporative Se losses between 23 to 51 % with $\delta^{82/76}$Se values ranging between 2.20 ± 0.20 ‰ and 3.20 ± 0.20 ‰ were determined by the double spike measurements (Fig. 1b, filled circles).

The data of our two experiments cannot be explained by a single unidirectional fractionation process as they do not fit a single Rayleigh evaporation function. The data rather indicate Rayleigh distillations with variable isotopic fractionations $\Delta_{vapor\text{-}solution}$ ranging between 3 and 12 ‰ (Fig. 1b). If the theoretical fractionation associated with evaporation corresponds to the square root of the evaporated molecule masses (Richter, 2004; Young et al., 2002), the inferred fractionations seem consistent with evaporation of pure $SeCl_2$ (fractionation $\Delta_{vapor\text{-}solution}$ of ~ 13 ‰) and pure $SeCl_6$ (fractionation $\Delta_{vapor\text{-}solution}$ of ~ 7 ‰). Future studies are needed to evaluate the exact speciation of evaporated selenium species. The origin of evaporative loss of Se remains unclear, but our experiments clearly demonstrate a significant loss of preferentially isotopically light Se during evaporation of pure reference materials. However, the double spike approach inherently corrects for such chemistry-induced fractionations.

2.4 Mass spectrometry (MC-ICP-MS)

Instrumental parameters and set up

Isotope measurements were conducted on a ThermoFisher Scientific® Neptune*Plus*™ multi-collector inductively coupled plasma mass spectrometer linked with a CETAC® HGX 200 hydride generator, an ESI MP2-6 peristaltic pump and an ESI SC-μ DX autosampler. To obtain the highest Se sensitivity at high front vacuum a nickel skimmer cone (H-cone) and a Ni-Jet sample cone were employed. Daily tuning included the gas flows and torch positions. Typical parameters and settings are listed in Table 2.

Measured masses include interference monitors for hydrides and argon dimers as generated in the plasma (Table 3). Signal intensities given in V are obtained using amplifier resistors of 10^{11} Ω.

[TABLE 2]

Hydride generation

One of the major advantages of a hydride introduction system is the efficient transport of Se into the plasma under dry conditions (Johnson and Bullen, 2004). The hydride generator serves as Se signal booster and as a purification device, because exclusively hydride-forming elements (e.g. Se, As, Ge) are effectively transferred to the plasma (Clark and Johnson, 2008). A sodium borohydride solution is prepared by adding 1 g of $NaBH_4$ (analysis grade) to 250 ml of 18.2MΩ-grade water. To stabilize the solution, 1 g of sodium hydroxide monohydrate is added. In our setup, constant flows of 2 mol L^{-1} HCl and sodium borohydride (NaBH4; 0.4 % (m/m)) are mixed in a coil which results in a steady production of hydrides throughout an entire measurement session. To this constant hydride-generating mixture the sample is then additionally introduced in 2 mol L^{-1} HCl and H_2Se is formed according to reaction (1) that can be ionized efficiently.

$$4\ H_2SeO_{3(aq)} + 3\ HCl_{(aq)} + 3\ NaBH_{4(aq)} \rightarrow 4\ H_2Se_{(g)} + 3\ H_3BO_{3(aq)} + 3\ H_2O + 3NaCl_{(aq)} \quad (1)$$

Residual non-hydride forming matrix elements that remain in the sample solution after chemical purification are fully excluded via a gas/liquid separator while hydrides are carried to the plasma in an argon flux (Fig. 2). In addition to argon for the plasma and to act as the sample carrier gas, we also introduced methane because it enhances the sensitivity for Se as shown in previous studies (e.g. Floor et al., 2011). In our instrumental setup, an increase of the Se signal by a factor two to three was achieved.

[FIGURE 2]

Analyses, interference corrections and double spike deconvolution

Instrument parameters were optimized for high Se signal intensities and low Argon dimers before each measurement session. Typical signals on ^{82}Se of a 15 ppb solution with the operating conditions summarized in Table 2 are 0.5 V. Each measurement consists of 40 cycles with 4.194 s integration time. Washout time was generally set to 4 minutes. All measurements of standards and samples were bracketed by background (on-peak zero) measurements of the same batch of pure 2 mol L^{-1} HCl in which standards and samples were taken up. On-peak zeros were subtracted from measured intensities of

standards and samples. Measurements of NIST SRM-3149 standard solutions were performed between each sample to assess potential instrumental drift. Additionally, standard solution MH-495 was measured after every 5th sample. Following acquisition of isotope signal intensities the data was further reduced offline. A major issue of stable Se isotope measurements are the numerous single-mass polyatomic isobaric interferences that typically form in plasma source mass spectrometers in the mass range of Se isotopes and interference monitors (Table 3). These spectral interferences can be divided into (i) plasma induced, (ii) plasma and analyte matrix induced and (iii) analyte and sample matrix induced.

[TABLE 3]

The subtraction of on-peak zero signals determined on pure analyte matrix solutions (i.e. 2 mol L^{-1} HCl) from sample signals adequately accounts for the small interferences of Kr and ArCl. On-peak zero subtraction, however, does not allow accurate correction of the large ArAr interferences due to the considerable fluctuations in the plasma energy between and within sample runs. We typically observe $^{40}Ar^{40}Ar^{+}$ signals of 20-25 V, with variations of this signal from scan to scan of ± 0.15 V due to plasma fluctuations. We therefore employed a two-step strategy for accurate correction of Ar dimer interferences:

(1) We admixed methane to the sample Ar gas carrying the SeH_2 from the hydride generator to the plasma torch (Fig. 2). Enhancement of Se signal and suppression of polyatomic interferences by methane addition for Se concentration and isotope ratio measurements has been described in previous studies (Fliegel et al., 2011; Floor et al., 2011; Guo et al., 2013). We indeed observed an approximately two- to three-fold increase in Se signal intensities and a decrease in Ar dimer intensities by a factor of two with an addition of 2.0 - 3.5 mL min^{-1} methane to the instrument. This significantly suppressed Ar dimer signals allowed more accurate on-peak zero corrections of polyatomic Ar interferences. Furthermore, hydride interferences ($ArArH^{+}$, SeH^{+}, GeH^{+}, BrH^{+}, AsH^{+}) dropped to negligible levels by methane addition making subsequent correction of hydrides after on-peak zero subtraction unnecessary.

(2) We employed a secondary correction for Ar dimer interferences as described by Elwaer and Hintelmann (2008), which takes plasma energy fluctuations into account. We used the ^{82}Se signal to predict the ^{80}Se signal of the samples by artificially fractionating the $^{82}Se/^{80}Se$ ratio using the samples'

instrumental mass bias. Assuming IUPAC Se isotope composition (Berglund and Wieser, 2011) the ^{80}Se signal of the sample is estimated and subtracted from the signal measured at m/z = 80 to estimate the excess or deficit in $^{40}Ar^{40}Ar^{+}$ compared to the on-peak zero measurement. Signals of the minor Ar dimers (i.e. $^{36}Ar^{36}Ar^{+}$, $^{38}Ar^{36}Ar^{+}$, $^{38}Ar^{38}Ar^{+}$, $^{40}Ar^{36}Ar^{+}$ and $^{40}Ar^{38}Ar^{+}$) are then determined relative to the calculated $^{40}Ar^{40}Ar^{+}$ signal considering the relative abundance of Ar isotopes (Berglund and Wieser, 2011). For measurements on 15 ng mL^{-1} sample solutions this correction improves the external 2σ reproducibility on $\delta^{82/76}Se$ values by 20 to 30 %. We tested the necessity to artificially fractionate Ar isotope ratios to account for the instrumental mass bias. We assumed that at a first order, Ar and Se are subject to equal isotope fractionations in the instrument plasma, which per se is not entirely correct. Since this artificial fractionation of Ar isotope ratios only resulted in shifts of 0.001 to 0.002 ‰ for both sample and standard solutions. This therefore means that the possible occurrence of Ar isotopic fractionation in the plasma has a negligible effect on our Se isotope data correction. Consequently, for routine measurements, possible Ar isotopic fractionations were ignored. The calculated ArAr interferences were arithmetically subtracted from measured Se signal intensities.

The iterative double spike deconvolution calculations used first by Compston and Oversby (1969) for Pb isotopes were applied to correct the measured Se isotope data with the exception that exponential rather than linear law was used as a proxy for the instrumental mass bias. Apart from the two spike isotopes ^{74}Se and ^{77}Se, ^{78}Se and ^{82}Se were used for the deconvolution. All isobaric interferences (e.g. Ge correction, see below) and the fluctuations of Ar dimers were iteratively converged within the double spike deconvolution for accurate corrections. The double spike deconvolution yields three types of information: (i) an exponential fractionation factor (per amu) for the instrumental mass bias, which might also include a mass-dependent Se isotope fractionation during chemical purification of the sample. (ii) An exponential fractionation (per amu) for the samples' natural mass-dependent fractionation compared to NIST SMR-3149 against which the double spike was calibrated. From this factor the samples' natural Se isotope ratios are calculated and can be reported in the δ-notation as the per mil difference in these ratios compared to that of the isotopically certified reference material NIST SRM-3149. The samples' natural isotope ratios are calculated according to

equation (2) and can be converted to any ratio per amu as a function of the exact masses of ^{82}Se, ^{78}Se and ^{76}Se (Young et al., 2002).

$$\delta^{82/78}Se = [(^{82}Se/^{78}Se)_{sample}/(^{82}Se/^{78}Se)_{NIST\ SRM\text{-}3149} - 1] \times 1000 \quad (2)$$

(iii) The spike-to-sample ratio from which, knowing the Se concentration of the double spike, an accurate Se concentration for the sample can be calculated.

Accuracy of isobaric interference correction of 74Ge on 74Se

Germanium like Se forms hydrides (GeH_4) leading to isobaric interferences of ^{74}Ge on ^{74}Se and ^{76}Ge on ^{76}Se during mass spectrometric analyses. We observed the Ge correction to be unnecessary if the measured Ge/Se ratio is smaller than 0.0001 when measuring 15 ng mL^{-1} sample solutions: below this threshold, Ge signals are below 0.5 mV on mass 72 and appear to be indistinguishable from background noise. Correcting for this signal only adds uncertainty to the internal precision of the $\delta^{82/76}Se$ value without significantly changing it. At Ge/Se ratios above this threshold value, the canonical $^{72}Ge/^{74}Ge$ ratio of 0.7521 (Berglund and Wieser, 2011) was artificially fractionated using the instrumental mass bias determined for Se to correct ^{74}Se from the isobaric interference of ^{74}Ge. However, the instrumental mass bias for Se also includes the mass-dependent Se isotope fractionation induced by the chemical purification when Se recovery is incomplete. Furthermore, the chemically induced mass-dependent isotope fractionation of Ge is likely different from that of Se. As a result, this correction is only applied to Ge/Se ratios < 0.0056. We set this value as it still yields accurate data for Se mass bias corrected data. Above this upper threshold value for the Ge/Se ratio (see. Fig. 3) for 15 ng mL^{-1} measurement solutions, signal intensities of ^{72}Ge and ^{73}Ge become large enough (> 2 mV on mass 72) to accurately determine the mass-dependent instrumental mass bias and chemical fractionation of Ge assuming a canonical $^{72}Ge/^{73}Ge$ of 0.2823 (Berglund and Wieser, 2011). To test the accuracy of our Ge interference correction method, 15 ng mL^{-1} NIST SRM-3149 solutions were mixed with different amounts of a pure Ge in-house standard solution, similar to a previous approach described by Pogge von Strandmann et al. (2014). As illustrated in Fig. 3 the values of the Ge-doped NIST SRM-3149 solutions perfectly lie within the external reproducibility for this standard of 0.00 ± 0.11 ‰ to Ge/Se ratios of up to 4, showing that this method accurately corrects any Ge interference.

[FIGURE 3]

3 Results and discussion

3.1 Se isotope measurements of matrix-free standard solutions

Background or "on-peak zero" (OPZ) corrections have been used in Se isotope analytical studies to account for plasma and other instrumental interferences (e.g. Johnson, 2004; Rouxel et al., 2002; Zhu et al., 2008). Previously performed scans on an Element 2 ICP-MS at high resolution ($M/\Delta M = \sim 10000$, 5 - 95 % peak edge width) resolved Se and ArAr peaks and observed constant voltage on ArAr peaks regardless of whether Se was introduced in the plasma (Pogge von Strandmann et al., 2014). This was argued to justify the use of OPZ correction. We performed Se isotopic measurements while using the OPZ correction on our MC-ICP-MS in low (LR) and medium resolution (MR) mode ($M/\Delta M = \sim 2000$ vs. MR: $M/\Delta M = \sim 7000$, respectively, 5 - 95 % peak edge width). The MR measurements allow crude resolution of Se and ArAr peaks but yielded indistinguishable isotope results than in LR mode. This confirms the validity of the OPZ correction and demonstrates that measurements in LR produce precise and accurate data as previously suggested (Pogge von Strandmann et al., 2014).

Over a period of over 6 months that included LR and MR measurements, a long-term average and reproducibility for MH-495 of $\delta^{82/76}Se = -3.27 \pm 0.13$ ‰ (2σ, n = 100) is obtained (Fig. 4). This is consistent with recently published values following double-spike measurements (-3.44 ± 0.06 ‰; 2σ, n = 5) (Zhu et al., 2014) and within uncertainty of an earlier study using standard-sample bracketing measurements (-3.04 ± 0.50 ‰, 2σ, n = 2) (Carignan and Wen, 2007).

[FIGURE 4]

3.2 Accuracy tests

Despite a quantitative removal of matrix elements by ion exchange chromatography and hydride generation, potential matrix effects may not be always ruled out because droplets from excess liquid could occasionally pass the PTFE-membrane of the hydride generation system. Although negligible voltages were observed on the masses of chloride (^{35}Cl and ^{37}Cl), the likely main constituent of such droplets, we tested the effect of variable matrix/Se ratios by adapting a standard addition method employed previously (Nielsen et al., 2004; Schumann et al., 1992; Tipper et al., 2008). Increasing amounts of MH-495 were admixed to constant amounts of NIST SRM-3149, homogenized (see section

356 2.3), re-dissolved and measured. Unresolved polyatomic interferences from the carrier solutions and/or
357 gases would lead to samples arbitrarily plotting off a two-component mixing line. Here we show that
358 mixtures remain within uncertainty of 0.20 ‰ (2σ) (Fig. 5a), which argues against the contribution of
359 unresolved interferences.

360 In addition, we performed accuracy tests involving USGS reference material SGR-1. Increasing
361 amounts of SGR-1 (20 to 40 mg or 70 to 140 ng total Se) were mixed to given amounts of standard
362 solution MH-495. Measured and calculated Se isotope compositions remain within uncertainty of
363 0.20 ‰ (2σ) and confirm that potential matrix-induced interferences are negligible (Fig. 5b).

364 **[FIGURE 5]**

365 3.3 Exploring the minimum Se required for accurate isotope measurements

366 A major goal is to determine Se isotope compositions of samples with low Se concentrations such as
367 basalts (< 200 ng g^{-1}, see below). Before this is attempted, the minimum Se required for measurement
368 was evaluated in a first step by analyzing 1 mL solutions of 50 to 3 ng per mL of MH-495 standard
369 solution (filled circles in Fig. 6). Measured signals on ^{82}Se ranged from 0.1 to 1.5 V and showed no
370 correlation with $\delta^{82/76}Se$ of MH-495. It is however observed that the uncertainties vary with signal
371 intensities: Solutions with a minimum of 15 ng mL^{-1} concentrations and > 0.5 V on mass ^{82}Se (lowest
372 abundant mass measured) show internal errors of 0.04 ‰ (2 s.e., n = 6) and yield an external
373 reproducibility of 0.09 ‰ (2σ, n = 6). Solutions between 15 and 7.5 ng mL^{-1} show a higher internal error
374 of up to 0.08 ‰ (2 s.e., n = 5) and the external reproducibility increases to 0.12 ‰ (2σ, n = 5). When
375 the ^{82}Se signal is below 0.18 V, equivalent to solutions below 7.5 ng mL^{-1}, the internal error increases
376 to 0.12 ‰ (2 s.e., n = 7) and the external reproducibility becomes > 0.20 ‰ (2σ, n = 7). Hence, the
377 external reproducibility systematically changes at a concentration of approximately 7.5 ng mL^{-1}. While
378 it is desirable to measure sample solutions with higher than 15 ng total Se, we show the instrumental
379 capability to yield 0.24 ‰ (2σ, n = 7) external reproducibility for down to 3 ng total Se. This is similar
380 to results of a previous study by Zhu et al. (2008) using a different set up.

381 **[FIGURE 6]**

382 Analogue to measurements of various amounts of MH-495 we performed tests with USGS
383 reference material SGR-1 (unfilled circles in Fig. 6). This involved the digestion of 100 mg SGR-1
384 (equivalent to ~ 350 ng total Se, section 2.2) and dilution to various concentrations (from 50 ng mL^{-1} to
385 5 ng mL^{-1}). As for standard solution MH-495, the internal errors and the external reproducibility depend
386 on signal intensities. Again, total Se contents with a minimum of 15 ng mL^{-1} yield internal errors of
387 0.04 ‰ (2 s.e., n = 4) and an external reproducibility of 0.06 ‰ (2σ, n = 4), whereas down to
388 7.5 ng mL^{-1} total Se analyzed yield internal errors of 0.07 ‰ (2 s.e., n = 4) and an external
389 reproducibility of 0.14 ‰ (2σ, n = 4). Below 7.5 ng mL^{-1} the ^{82}Se signal intensities are < 0.18 V and the
390 internal error increases to 0.10 ‰ (2 s.e., n = 6) and the external reproducibility is > 0.14 ‰.
391 This reproducibility obtained with a NeptunePlus™ instrument is similar to that previously
392 reported for other instruments where similarly small quantities were analyzed (5 ng total Se analyzed
393 with 0.25 ‰ (2σ) on $\delta^{82/76}Se$ on a Micromass IsoProbe by Rouxel et al. (2002) and on a NuPlasma by
394 Zhu et al. (2008) (4 ng total Se analyzed with 0.10 ‰ (2σ) for standard solutions MH 495 and
395 NIST SRM-3149 and 0.15 - 0.20 ‰ (2σ) for natural samples).
396 Measurements of USGS reference shales (SGR-1 and SCo-1) allow comparison to previous
397 studies (Kipp et al., 2017; Mitchell et al., 2012; Pogge von Strandmann et al., 2014; Pogge von
398 Strandmann et al., 2015; Rouxel et al., 2002; Schilling et al., 2011; Stüeken et al., 2013; Stüeken et al.,
399 2015b; Stüeken et al., 2015c; Vollstaedt et al., 2016a) and have relatively high Se abundances (SGR-
400 1: 3.50 ± 0.28 $\mu g\ g^{-1}$; SCo-1: 0.89 ± 0.06 $\mu g\ g^{-1}$) (Gladney and Roelandts, 1988).
401 Both our obtained concentrations (SGR-1: 3.76 ± 0.32 $\mu g\ g^{-1}$, 2σ, n = 9;
402 SCo-1: 0.84 ± 0.06 $\mu g\ g^{-1}$, 2σ, n = 5) and isotopic compositions (SGR-1: -0.08 ± 0.20 ‰, 2σ, n = 9;
403 SCo-1: -0.18 ± 0.22 ‰, 2σ, n = 5) are within error of most previous studies (see Fig. 7) (Kipp et al.,
404 2017; Mitchell et al., 2012; Pogge von Strandmann et al., 2014; Rouxel et al., 2002; Savard et al., 2009;
405 Schilling et al., 2011; Stüeken et al., 2013; Stüeken et al., 2015b; Stüeken et al., 2015c; Vollstaedt et al.,
406 2016a) and demonstrate full homogenization of sample with double spike Se. The USGS SGR-1 batch
407 (USGS SGR-1, Split 25, Position 8) used in this study may be affected by heterogeneity. This may
408 explain better reproducibility for repeated isotope measurements on diluted solutions from the same
409 sample digestion, compared to solutions from separately digested material. Therefore, our values for

410 samples (Fig. 7 and Tab. 4) that were obtained from separately digested material in different
411 measurement sessions over a period of 9 months provide a long-term external reproducibility.

412 **[FIGURE 7]**

413 **[TABLE 4]**

414 3.4 Selenium measurements of samples with concentrations in the ng g^{-1} range

415 In order to test our method on low Se containing samples with a matrix relevant to mantle derived rocks,
416 USGS reference basalt BCR-2 is suitable (78 ± 3.2 ng g^{-1}, 1σ, n = 5) (Lissner et al., 2014). For this we
417 weighted, double-spiked and digested 300 mg of BCR-2 (equivalent to ca. 25 ng total Se). Our batch of
418 BCR-2 (3223) yields a Se concentration of 71 ± 4 ng g^{-1} (1σ, n = 3, Tab. 4), which is within uncertainty
419 to published concentrations (Lissner et al., 2014). The isotopic data acquired is based on measurements
420 of 1 mL sample solution containing ca. 15 ng total Se. Our measurement yields $\delta^{82/76}$Se of 0.18 ± 0.03 ‰
421 (2σ, n = 3). This value is also within uncertainty to 0.24 ± 0.25 ‰ (2σ, n = n. g.) reported by Rouxel et
422 al. (2002). It is important to note that the isotopic composition obtained is unlikely to represent a mantle
423 reference value as mantle processes are not entirely understood yet. The pioneering study by Rouxel et
424 al. (2002) reported a large variety of different geological materials. It is also noteworthy that accurate
425 stable Se isotope measurements down to the lower ng level have been reported by (Zhu et al., 2008).
426 Both groups however reported Se isotope data from analysis on different instruments compared to a
427 Neptune*Plus*™. While Zhu et al. (2008) and further colleagues of Prof. T. Johnson at the Department of
428 Geology, University of Illinois at Urbana-Champaign (e.g. Mitchell et al., 2012; Schilling et al., 2011)
429 analyzed Se isotopes on a NuPlasma, Rouxel et al. (2002) used a Micromass IsoProbe plasma source
430 instrument with collision/reaction cell technology, which suppressed the formation of polyatomic
431 interferences down to insignificant levels. However, neither this instrument nor another MC-ICP-MS
432 with collision/reaction cell technology are commercially available at the present. The ThermoFisher
433 Scientific® Neptune*Plus*™ used in this study could be used in medium- or high-mass resolution mode,
434 as a strategy to resolve polyatomic interferences from monoatomic ion beams at a given m/z ratio
435 (Weyer and Schwieters, 2003). Unfortunately, this technique clips the ion beam leading to a significant
436 decrease in ion beam intensity to 15 % for medium- and to 8 % for high-mass resolution compared to

437 the normal low-mass resolution measurement mode. In medium- or high-resolution modes, it is thus
438 impossible to obtain accurate Se isotope compositions on analytes with lower than 15 ng total Se, even
439 with the efficient sample introduction to the plasma promoted by a hydride generator. At a low-mass
440 resolution measurement mode on the Neptune*Plus*™ MC-ICP-MS, however, background signals mainly
441 from Ar dimers are in the range of tens of mV at m/z of 74, 77, 78 and 82 and are very large (20 - 25 V)
442 at m/z of 80 (i.e. $^{40}Ar/^{40}Ar^{+}$) using amplifier resistors of 10^{11} Ω. In comparison, Rouxel et al. (2002) only
443 report background levels on their Micromass Isoprobe at m/z = 80 to be < 1 mV (using a 10^{11} Ω amplifier
444 resistor). Here, we report the first Se measurement method on the ThermoFisher Scientific®
445 Neptune*Plus*™ MC-ICP-MS that minimizes the problem of major polyatomic interferences on Se isotope
446 masses by introducing methane. Together with a hydride generation system, this additionally increases
447 the Se signal and thus enables the measurement of materials with Se concentrations in the range of 15 ng
448 with a 2σ reproducibility of ca. 0.10 ‰ and of 5 ng with a reproducibility of 0.20 ‰. This is significant
449 because it allows a systematic Se isotope investigation of many planetary reservoirs such as the Earth's
450 mantle, which is characterized by low Se concentrations (peridotites: ~ 1 - 150 ng g^{-1} (König et al.,
451 2014); MORB: 120 - 200 ng g^{-1} (Lissner et al., 2014)) as well as different sulfides and minerals (e.g.
452 mantle sulfides range from 20 to 280 μg g^{-1}-Se (e.g. Hattori et al., 2002)).

453 # 4 Conclusions

454 (1) The method presented here allows to employ a ThermoFisher Scientific® Neptune*Plus*™ for the
455 accurate determination of Se isotope ratios. The method is based on a double spike to account
456 for fractionation induced during all stages of sample preparation and combines hydride
457 generation with the introduction of methane, which results in a two- to three-fold Se signal
458 increase and background suppression by a factor of two.
459 (2) Accurate Se isotope measurements with a reproducibility of < 0.10 ‰ (2σ) on $\delta^{82/76}$Se are
460 obtained on 1 mL sample solution with a total of 15 ng Se. With lower Se quantities down to
461 5 ng mL^{-1} a reproducibility of 0.20 ‰ (2σ) is obtained on $\delta^{82/76}$Se.
462 (3) Our analytical approach for Se isotope analysis pushes the boundary for the investigation of
463 geological materials and single minerals with low Se concentrations (200 ng g^{-1} down to tens of

464 ng g^{-1}) and thus allows investigating Se-depleted planetary reservoirs such as the terrestrial
465 mantle and other high-temperature environments by employing a commercially available
466 instrument, the ThermoFisher Scientific® Neptune*Plus*™ MC-ICP-MS. As a first result we
467 report a $\delta^{82/76}$Se value of 0.18 ± 0.03 ‰ (2σ; n = 3) for the USGS reference basalt BCR-2. This
468 value should not be regarded as mantle reference value as processes in the Earth's mantle that
469 might produce Se isotopic fractionations cannot be ruled out.

470

471 *Acknowledgements*: - This work was funded by an ERC Starting Grant (O2RIGIN, 636808) to Stephan
472 König. We thank Thomas M. Johnson for providing reference solution MH-495. Elmar Reitter and
473 Martin Wille provided significant laboratory and instrumental support and contributed to fruitful
474 discussions. Eva Stüeken, Hauke Vollstaedt and Philip A. E. Pogge von Strandmann are thanked for
475 constructive reviews which helped to improve the manuscript.

476 References

477 Alard, O., Lorand, J.-P., Reisberg, L., Bodinier, J.-L., Dautria, J.-M., O'Reilly, S.Y., 2011. Volatile-rich
478 Metasomatism in Montferrier Xenoliths (Southern France): Implications for the Abundances of
479 Chalcophile and Highly Siderophile Elements in the Subcontinental Mantle. Journal of
480 Petrology, 52(10): 2009-2045.

481 Becker, H., Horan, M.F., Walker, R.J., Gao, S., Lorand, J.P., Rudnick, R.L., 2006. Highly siderophile
482 element composition of the Earth's primitive upper mantle: Constraints from new data on
483 peridotite massifs and xenoliths. Geochimica Et Cosmochimica Acta, 70(17): 4528-4550.

484 Berglund, M., Wieser, M.E., 2011. Isotopic compositions of the elements 2009 (IUPAC Technical
485 Report). Pure and Applied Chemistry, 83(2).

486 Brenan, J.M., 2015. Se–Te fractionation by sulfide–silicate melt partitioning: implications for the
487 composition of mantle-derived magmas and their melting residues. Earth and Planetary Science
488 Letters, 422: 45-57.

489 Carignan, J., Wen, H., 2007. Scaling NIST SRM 3149 for Se isotope analysis and isotopic variations of
490 natural samples. Chemical Geology, 242(3–4): 347-350.

491 Clark, S.K., Johnson, T.M., 2008. Effective isotopic fractionation factors for solute removal by reactive
492 sediments: A laboratory microcosm and slurry study. Environmental science & technology,
493 42(21): 7850-7855.

494 Clark, S.K., Johnson, T.M., 2010. Selenium Stable Isotope Investigation into Selenium Biogeochemical
495 Cycling in a Lacustrine Environment: Sweitzer Lake, Colorado. Journal of Environment
496 Quality, 39(6): 2200.

497 Compston, W., Oversby, V., 1969. Lead isotopic analysis using a double spike. Journal of Geophysical
498 Research, 74(17): 4338-4348.

499 Ellis, A.S., Johnson, T.M., Herbel, M.J., Bullen, T.D., 2003. Stable isotope fractionation of selenium by
500 natural microbial consortia. Chemical geology, 195(1): 119-129.

501 Elwaer, N., Hintelmann, H., 2008. Selective separation of selenium (IV) by thiol cellulose powder and
502 subsequent selenium isotope ratio determination using multicollector inductively coupled
503 plasma mass spectrometry. Journal of Analytical Atomic Spectrometry, 23(5): 733-743.

504 Fehr, M.A., Rehkämper, M., Halliday, A.N., 2004. Application of MC-ICPMS to the precise
505 determination of tellurium isotope compositions in chondrites, iron meteorites and sulfides.
506 International Journal of Mass Spectrometry, 232(1): 83-94.

507 Fliegel, D., Frei, C., Fontaine, G., Hu, Z., Gao, S., Günther, D., 2011. Sensitivity improvement in laser
508 ablation inductively coupled plasma mass spectrometry achieved using a methane/argon and
509 methanol/water/argon mixed gas plasma. Analyst, 136(23): 4925-4934.

510 Floor, G.H., Millot, R., Iglesias, M., Négrel, P., 2011. Influence of methane addition on selenium isotope
511 sensitivity and their spectral interferences. Journal of Mass Spectrometry, 46(2): 182-188.

512 Gladney, E.S., Roelandts, I., 1988. 1987 Compilation of Elemental Concentration Data for USGS
513 BHVO-1, MAG-1, QLO-1, RGM-1, SCo-1, SDC-1, SGR-1 and STM-1. Geostandards
514 Newsletter, 12(2): 253-362.

Guo, W., Hu, S., Wang, Y., Zhang, L., Hu, Z., Zhang, J., 2013. Trace determination of selenium in biological samples by CH 4-Ar mixed gas plasma DRC-ICP-MS. Microchemical Journal, 108: 106-112.

Hattori, K.H., Arai, S., Clarke, D.B., 2002. Selenium, tellurium, arsenic and antimony contents of primary mantle sulfides. The Canadian Mineralogist, 40(2): 637-650.

Johnson, T.M., 2004. A review of mass-dependent fractionation of selenium isotopes and implications for other heavy stable isotopes. Chemical Geology, 204(3): 201-214.

Johnson, T.M., Bullen, T.D., 2003. Selenium isotope fractionation during reduction by Fe(II)-Fe(III) hydroxide-sulfate (green rust). Geochimica Et Cosmochimica Acta, 67(3): 413-419.

Johnson, T.M., Bullen, T.D., 2004. Mass-dependent fractionation of selenium and chromium isotopes in low-temperature environments. Reviews in mineralogy and geochemistry, 55(1): 289-317.

Johnson, T.M., Bullen, T.D., Zawislanski, P.T., 2000. Selenium stable isotope ratios as indicators of sources and cycling of selenium: Results from the northern reach of San Francisco Bay. Environmental science & technology, 34(11): 2075-2079.

Johnson, T.M., Herbel, M.J., Bullen, T.D., Zawislanski, P.T., 1999. Selenium isotope ratios as indicators of selenium sources and oxyanion reduction. Geochimica et Cosmochimica Acta, 63(18): 2775-2783.

Kimura, K., Lewis, R.S., Anders, E., 1974. Distribution of gold and rhenium between nickel-iron and silicate melts: implications for the abundance of siderophile elements on the Earth and Moon. Geochimica et Cosmochimica Acta, 38(5): 683-701.

Kipp, M.A., Stüeken, E.E., Bekker, A., Buick, R., 2017. Selenium isotopes record extensive marine suboxia during the Great Oxidation Event. Proceedings of the National Academy of Sciences, 114(5): 875-880.

König, S., Lissner, M., Lorand, J.-P., Bragagni, A., Luguet, A., 2015a. Mineralogical control of selenium, tellurium and highly siderophile elements in the Earth's mantle: Evidence from mineral separates of ultra-depleted mantle residues. Chemical Geology, 396: 16-24.

König, S., Lorand, J.-P., Luguet, A., Pearson, D.G., 2014. A non-primitive origin of near-chondritic S–Se–Te ratios in mantle peridotites; implications for the Earth's late accretionary history. Earth and Planetary Science Letters, 385: 110-121.

König, S., Luguet, A., Lorand, J.-P., Lissner, M., Graham Pearson, D., 2015b. Reply to the comment on "A non-primitive origin of near-chondritic S–Se–Te ratios in mantle peridotites: Implications for the Earth's late accretionary history" by König S. et al. [Earth Planet. Sci. Lett. 385 (2014) 110–121]. Earth and Planetary Science Letters, 417: 167-169.

König, S., Luguet, A., Lorand, J.-P., Wombacher, F., Lissner, M., 2012. Selenium and tellurium systematics of the Earth's mantle from high precision analyses of ultra-depleted orogenic peridotites. Geochimica et Cosmochimica Acta, 86: 354-366.

Layton-Matthews, D., Leybourne, M.I., Peter, J.M., Scott, S.D., 2006. Determination of selenium isotopic ratios by continuous-hydride-generation dynamic-reaction-cell inductively coupled plasma-mass spectrometry. Journal of Analytical Atomic Spectrometry, 21(1): 41-49.

Lissner, M., König, S., Luguet, A., le Roux, P., Schuth, S., Heuser, A., le Roex, A., 2014. Selenium and tellurium systematics in MORBs from the southern Mid-Atlantic Ridge (47–50 S). Geochimica et Cosmochimica Acta, 144: 379-402.

Lorand, J.-P., Alard, O., 2010. Determination of selenium and tellurium concentrations in Pyrenean peridotites (Ariege, France): new insight into S/Se/Te systematics of the upper in mantle samples. Chemical Geology, 278(1): 120-130.

Lorand, J.-P., Alard, O., Luguet, A., Keays, R.R., 2003. Sulfur and selenium systematics of the subcontinental lithospheric mantle: inferences from the Massif Central xenolith suite (France). Geochimica et Cosmochimica Acta, 67(21): 4137-4151.

563 Lorand, J.-P., Delpech, G., Grégoire, M., Moine, B., O'Reilly, S.Y., Cottin, J.-Y., 2004. Platinum-group
564 elements and the multistage metasomatic history of Kerguelen lithospheric mantle (South Indian
565 Ocean). Chemical Geology, 208(1–4): 195-215.

566 Lorand, J.-P., Luguet, A., Alard, O., 2013. Platinum-group element systematics and petrogenetic
567 processing of the continental upper mantle: A review. Lithos, 164–167: 2-21.

568 Lorand, J.-P., Luguet, A., Alard, O., Bezos, A., Meisel, T., 2008. Abundance and distribution of
569 platinum-group elements in orogenic lherzolites; a case study in a Fontete Rouge lherzolite
570 (French Pyrénées). Chemical Geology, 248(3–4): 174-194.

571 Luguet, A., Lorand, J.-P., Alard, O., Cottin, J.-Y., 2004. A multi-technique study of platinum group
572 element systematic in some Ligurian ophiolitic peridotites, Italy. Chemical Geology, 208(1–4):
573 175-194.

574 Mann, U., Frost, D.J., Rubie, D.C., Becker, H., Audétat, A., 2012. Partitioning of Ru, Rh, Pd, Re, Ir and
575 Pt between liquid metal and silicate at high pressures and high temperatures-Implications for
576 the origin of highly siderophile element concentrations in the Earth's mantle. Geochimica et
577 Cosmochimica Acta, 84: 593-613.

578 Marchesi, C., Garrido, C.J., Harvey, J., González-Jiménez, J.M., Hidas, K., Lorand, J.-P., Gervilla, F.,
579 2013. Platinum-group elements, S, Se and Cu in highly depleted abyssal peridotites from the
580 Mid-Atlantic Ocean Ridge (ODP Hole 1274A): Influence of hydrothermal and magmatic
581 processes. Contributions to Mineralogy and Petrology, 166(5): 1521-1538.

582 Marin, L., Lhomme, J., Carignan, J., 2001. Determination of selenium concentration in sixty five
583 reference materials for geochemical analysis by GFAAS after separation with thiol cotton.
584 Geostandards Newsletter, 25(2-3): 317-324.

585 McDonough, W.F., Sun, S.-S., 1995. The composition of the Earth. Chemical Geology, 120: 223-253.

586 Mitchell, K., Couture, R.-M., Johnson, T.M., Mason, P.R., Van Cappellen, P., 2013. Selenium sorption
587 and isotope fractionation: Iron (III) oxides versus iron (II) sulfides. Chemical Geology, 342: 21-
588 28.

589 Mitchell, K., Mansoor, S.Z., Mason, P.R.D., Johnson, T.M., Van Cappellen, P., 2016. Geological
590 evolution of the marine selenium cycle: Insights from the bulk shale δ82/76Se record and
591 isotope mass balance modeling. Earth and Planetary Science Letters, 441: 178-187.

592 Mitchell, K., Mason, P.R., Van Cappellen, P., Johnson, T.M., Gill, B.C., Owens, J.D., Diaz, J., Ingall,
593 E.D., Reichart, G.-J., Lyons, T.W., 2012. Selenium as paleo-oceanographic proxy: A first
594 assessment. Geochimica et Cosmochimica Acta, 89: 302-317.

595 Morgan, J., Walker, R., Brandon, A., Horan, M., 2001. Siderophile elements in Earth's upper mantle
596 and lunar breccias: data synthesis suggests manifestations of the same late influx. Meteoritics
597 & Planetary Science, 36(9): 1257-1275.

598 Morgan, J.W., 1986. Ultramafic xenoliths: clues to Earth's late accretionary history. Journal of
599 Geophysical Research: Solid Earth, 91(B12): 12375-12387.

600 Nielsen, S.G., Rehkämper, M., Baker, J., Halliday, A.N., 2004. The precise and accurate determination
601 of thallium isotope compositions and concentrations for water samples by MC-ICPMS.
602 Chemical Geology, 204(1-2): 109-124.

603 Palme, H., O'Neill, H.S.C., 2003. Cosmochemical estimates of mantle composition. Treatise on
604 geochemistry, 2: 568.

605 Pogge von Strandmann, P.A., Coath, C.D., Catling, D.C., Poulton, S.W., Elliott, T., 2014. Analysis of
606 mass dependent and mass independent selenium isotope variability in black shales. Journal of
607 Analytical Atomic Spectrometry, 29(9): 1648-1659.

608 Pogge von Strandmann, P.A., Stüeken, E.E., Elliott, T., Poulton, S.W., Dehler, C.M., Canfield, D.E.,
609 Catling, D.C., 2015. Selenium isotope evidence for progressive oxidation of the Neoproterozoic
610 biosphere. Nature communications, 6.

611 Richter, F.M., 2004. Timescales determining the degree of kinetic isotope fractionation by evaporation
612 and condensation. Geochimica et cosmochimica acta, 68(23): 4971-4992.

613 Rouxel, O., Fouquet, Y., Ludden, J.N., 2004. Subsurface processes at the lucky strike hydrothermal
614 field, Mid-Atlantic ridge: evidence from sulfur, selenium, and iron isotopes 1. Geochimica et
615 Cosmochimica Acta, 68(10): 2295-2311.

616 Rouxel, O., Ludden, J., Carignan, J., Marin, L., Fouquet, Y., 2002. Natural variations of Se isotopic
617 composition determined by hydride generation multiple collector inductively coupled plasma
618 mass spectrometry. Geochimica et Cosmochimica Acta, 66(18): 3191-3199.

619 Rudge, J.F., Reynolds, B.C., Bourdon, B., 2009. The double spike toolbox. Chemical Geology, 265(3):
620 420-431.

621 Savard, D., Bédard, L.P., Barnes, S.-J., 2009. Selenium Concentrations in Twenty-Six Geological
622 Reference Materials: New Determinations and Proposed Values. Geostandards and
623 Geoanalytical Research, 33(2): 249-259.

624 Schilling, K., Johnson, T.M., Mason, P.R.D., 2014. A sequential extraction technique for mass-balanced
625 stable selenium isotope analysis of soil samples. Chemical Geology, 381: 125-130.

626 Schilling, K., Johnson, T.M., Wilcke, W., 2011. Selenium partitioning and stable isotope ratios in urban
627 topsoils. Soil Science Society of America Journal, 75(4): 1354-1364.

628 Schilling, K., Johnson, T.M., Wilcke, W., 2013. Isotope fractionation of selenium by biomethylation in
629 microcosm incubations of soil. Chemical Geology, 352: 101-107.

630 Schumann, G., Klauke, R., Büttner, J., 1992. 036 Standard addition in HPLC: A calibration method for
631 the determination of reference method values. Fresenius' Journal of Analytical Chemistry,
632 343(1): 89-90.

633 Shore, A.J.T., 2011. Selenium geochemistry and isotopic composition of sediments from the Cariaco
634 Basin and the Bermuda Rise: a comparison between a restricted basin and the open ocean over
635 the last 500 ka, University of Leicester.

636 Stüeken, E., Foriel, J., Nelson, B., Buick, R., Catling, D., 2013. Selenium isotope analysis of organic-
637 rich shales: Advances in sample preparation and isobaric interference correction. Journal of
638 Analytical Atomic Spectrometry, 28(11): 1734-1749.

639 Stüeken, E.E., Buick, R., Anbar, A.D., 2015a. Selenium isotopes support free O2 in the latest Archean.
640 Geology, 43(3): 259-262.

641 Stüeken, E.E., Buick, R., Bekker, A., Catling, D., Foriel, J., Guy, B.M., Kah, L.C., Machel, H.G.,
642 Montanez, I.P., Poulton, S.W., 2015b. The evolution of the global selenium cycle: Secular
643 trends in Se isotopes and abundances. Geochimica Et Cosmochimica Acta, 162: 109-125.

644 Stüeken, E.E., Foriel, J., Buick, R., Schoepfer, S.D., 2015c. Selenium isotope ratios, redox changes and
645 biological productivity across the end-Permian mass extinction. Chemical Geology, 410: 28-39.

646 Tamari, Y., Ogawa, H., Fukumoto, Y., Tsuji, H., Kusaka, Y., 1990. Selenium Content and Its Oxidation-
647 State in Igneous Rocks, Rock-Forming Minerals, and a Reservoir Sediment. Bulletin of the
648 Chemical Society of Japan, 63(9): 2631-2638.

649 Tipper, E.T., Louvat, P., Capmas, F., Galy, A., Gaillardet, J., 2008. Accuracy of stable Mg and Ca
650 isotope data obtained by MC-ICP-MS using the standard addition method. Chemical Geology,
651 257(1-2): 65-75.

652 Vollstaedt, H., Mezger, K., Leya, I., 2016a. The isotope composition of selenium in chondrites
653 constrains the depletion mechanism of volatile elements in solar system materials. Earth and
654 Planetary Science Letters, 450: 372-380.

655 Vollstaedt, H., Mezger, K., Nagler, T., Leya, I., Trinquier, A., 2016b. Selenium isotope analysis by N-
656 TIMS: Potential and challenges. International Journal of Mass Spectrometry, 401: 55-63.

657 Walker, R.J., 2009. Highly siderophile elements in the Earth, Moon and Mars: Update and implications
658 for planetary accretion and differentiation. Chemie der Erde - Geochemistry, 69(2): 101-125.

659 Wang, Z., Becker, H., 2013. Ratios of S, Se and Te in the silicate Earth require a volatile-rich late veneer.
660 Nature, 499(7458): 328-331.

661 Wang, Z., Becker, H., 2015. Comment on "A non-primitive origin of near-chondritic SSeTe ratios in
662 mantle peridotites: Implications for the Earth's late accretionary history" by König S. et al.
663 [Earth Planet. Sci. Lett. 385 (2014) 110–121]. Earth and Planetary Science Letters, 417: 164-
664 166.

665 Wang, Z., Becker, H., Gawronski, T., 2013. Partial re-equilibration of highly siderophile elements and
666 the chalcogens in the mantle: A case study on the Baldissero and Balmuccia peridotite massifs
667 (Ivrea Zone, Italian Alps). Geochimica et Cosmochimica Acta, 108: 21-44.

668 Wen, H., Carignan, J., 2011. Selenium isotopes trace the source and redox processes in the black shale-
669 hosted Se-rich deposits in China. Geochimica et Cosmochimica Acta, 75(6): 1411-1427.

670 Wen, H., Carignan, J., Chu, X., Fan, H., Cloquet, C., Huang, J., Zhang, Y., Chang, H., 2014. Selenium
671 isotopes trace anoxic and ferruginous seawater conditions in the Early Cambrian. Chemical
672 Geology, 390: 164-172.

673 Weyer, S., Schwieters, J., 2003. High precision Fe isotope measurements with high mass resolution MC-
674 ICPMS. International Journal of Mass Spectrometry, 226(3): 355-368.

675 Young, E.D., Galy, A., Nagahara, H., 2002. Kinetic and equilibrium mass-dependent isotope
676 fractionation laws in nature and their geochemical and cosmochemical significance.
677 Geochimica et Cosmochimica Acta, 66(6): 1095-1104.

678 Yu, M.Q., Liu, G.Q., Jin, Q., 1983. Determination of trace arsenic, antimony, selenium and tellurium in
679 various oxidation states in water by hydride generation and atomic-absorption
680 spectrophotometry after enrichment and separation with thiol cotton. Talanta, 30(4): 265-70.

681 Zhu, J.-M., Johnson, T.M., Clark, S.K., Xiang-Kun, Z., 2008. High precision measurement of selenium
682 isotopic composition by hydride generation multiple collector inductively coupled plasma mass
683 spectrometry with a 74 Se-77 Se double spike. Chinese Journal of Analytical Chemistry, 36(10):
684 1385-1390.

685 Zhu, J.-M., Johnson, T.M., Clark, S.K., Zhu, X.-K., Wang, X.-L., 2014. Selenium redox cycling during
686 weathering of Se-rich shales: A selenium isotope study. Geochimica et Cosmochimica Acta,
687 126: 228-249.

688 Table captions:

689 Table 1: Overview of Se double spike compositions used by groups measuring on MC-ICP-MS.
690 Bold numbers indicate spike isotopes. Data acquisition at 1: Bristol Isotope Group, School
691 of Earth Sciences, Bristol University, UK. 2: Institute of Geological Sciences, University
692 of Bern, Switzerland. 3: Department of Geology, University of Illinois at Urbana-
693 Champaign, Urbana. 4 (this study): Isotope Geochemistry, University of Tübingen,
694 Germany.

695 Table 2: Operating parameters.

696 Table 3: Measured masses and associated isobaric interferences.

697 Table 4: Se isotope data for USGS reference materials SGR-1, SCo-1 and BCR-2.

698

699 Figure captions:

700 Fig. 1: (a) Measured $\delta^{82/76}Se_{NIST\ SRM\text{-}3149}$ as a function of various proportions of double spike (filled
701 circles). The results indicate that even significantly underspiked ($f_{spike} = 0.2$) or overspiked
702 ($f_{spike} = 0.8$) standards yield accurate data. Grey box represents the long-term average for
703 $\delta^{82/76}Se_{NIST\ SRM\text{-}3149}$ of 0.00 ± 0.11 ‰ (2σ, $n = 350$). Unfilled circles show measured
704 $\delta^{82/76}Se_{NIST\ SRM\text{-}3149}$ for unequilibrated mixtures of standard and double spike Se, resulting
705 in isotopic shift towards heavier values of 0.10 to 0.60 ‰. Error bars are internal errors
706 (2 s.e.) for each measurement. (b) $\delta^{82/76}Se_{NIST\ SRM\text{-}3149}$ as a function of evaporative loss of
707 light Se isotopes. Results indicate unpredictable loss-induced fractionation between

solution and vapor even at 65 °C and thus illustrate the requirement for double spike use in our experimental set up. Unfilled circles represent data from SSB measurements. Filled circles represent double spike measurements (section 2.3). Uncertainty on data is 0.20 ‰ (2σ). See section 2.3 for details.

Fig. 2: Schematic set up of the hydride generator system.

Fig. 3: Results of measurements of Se standard solution NIST SRM-3149 doped with different amounts of Ge. The constant range of $\delta^{82/76}Se$ shows efficient correction even for Ge/Se ratios of up to 4. Grey bar represents 2σ (0.08 ‰) of obtained $\delta^{82/76}Se_{NIST\ SRM\text{-}3149}$ data, whereas error bars are in-run errors (2 s.e.) of single measurements. Dashed lines indicate threshold values for correction with Se or Ge mass bias, respectively. Unfilled symbols indicate uncorrected $\delta^{82/76}Se_{NIST\ SRM\text{-}3149}$ (uncorrected data for Ge/Se > 0.0056 given in logarithmic scale as isotopic shift is > 1.3 to 1006 ‰).

Fig. 4: Long-term reproducibility of NIST SRM-3149 ($\delta^{82/76}Se_{NIST\ SRM\text{-}3149}$: 0.00 ± 0.11‰,n = 350) and MH-495 ($\delta^{82/76}Se_{NIST\ SRM\text{-}3149}$: -3.27 ± 0.13 ‰; n = 100). Grey bars represent 2σ uncertainties. Measurements in MR yield indistinguishable data compared to data acquired in LR, showing that LR measurements are sufficient for precise and accurate Se isotope data acquisition.

Fig. 5: Results for Se isotope measurements of mixtures between (a) standard solutions MH-495 and NIST SRM-3149 and (b) increasing amounts of sample SGR-1 (20 to 40 mg or 70 to 140 ng total Se) and constant amounts of standard solution MH-495. Doped solutions fall on a mixing line between endmembers within maximum uncertainty of 0.20 ‰ (2σ), indicating no bias despite increasing matrix over total Se and potential emergence of interferences above background. Endmember data taken from same measurement session.

Fig. 6: Results and signal-dependent external reproducibility for measurements of various dilutions of the MH-495 standard solution (filled circles) and 100 mg digested USGS rock reference material SGR-1 (unfilled circles). Error bars represent 2 standard errors (2 s.e.) of the individual measurements. Black dashed horizontal lines represent average value of dilutions > 7.5 ng mL^{-1} as these are characterized by decent internal errors. Black solid horizontal lines are 2σ uncertainties. Vertical dashed lines divide dilutions into < 7.5 ng mL^{-1}, 7.5 - 15 ng mL^{-1} and > 15 ng mL^{-1}, which are characterized by different internal errors (2 s.e) and external reproducibility (see section 3.3).

Fig. 7: Compiled Se isotope data for USGS shales SCo-1 and SGR-1. Filled symbols represent results from this study, combining 5 analytical sessions over a period of 9 months (SCo-1: -0.18 ± 0.22 ‰, n = 5; SGR-1: -0.08 ± 0.19 ‰, n = 11), providing a long-term external reproducibility for data obtained in our study. Unfilled symbols are data taken from the literature. All error bars indicate 2σ analytical reproducibility; errors where converted to 2σ where data was given in 1σ (e.g. Stüeken et al., 2013; 2015b, 2015c; Kipp et al., 2017). * = Data reported as $\delta^{82/78}Se$ was converted to $\delta^{82/76}Se$.

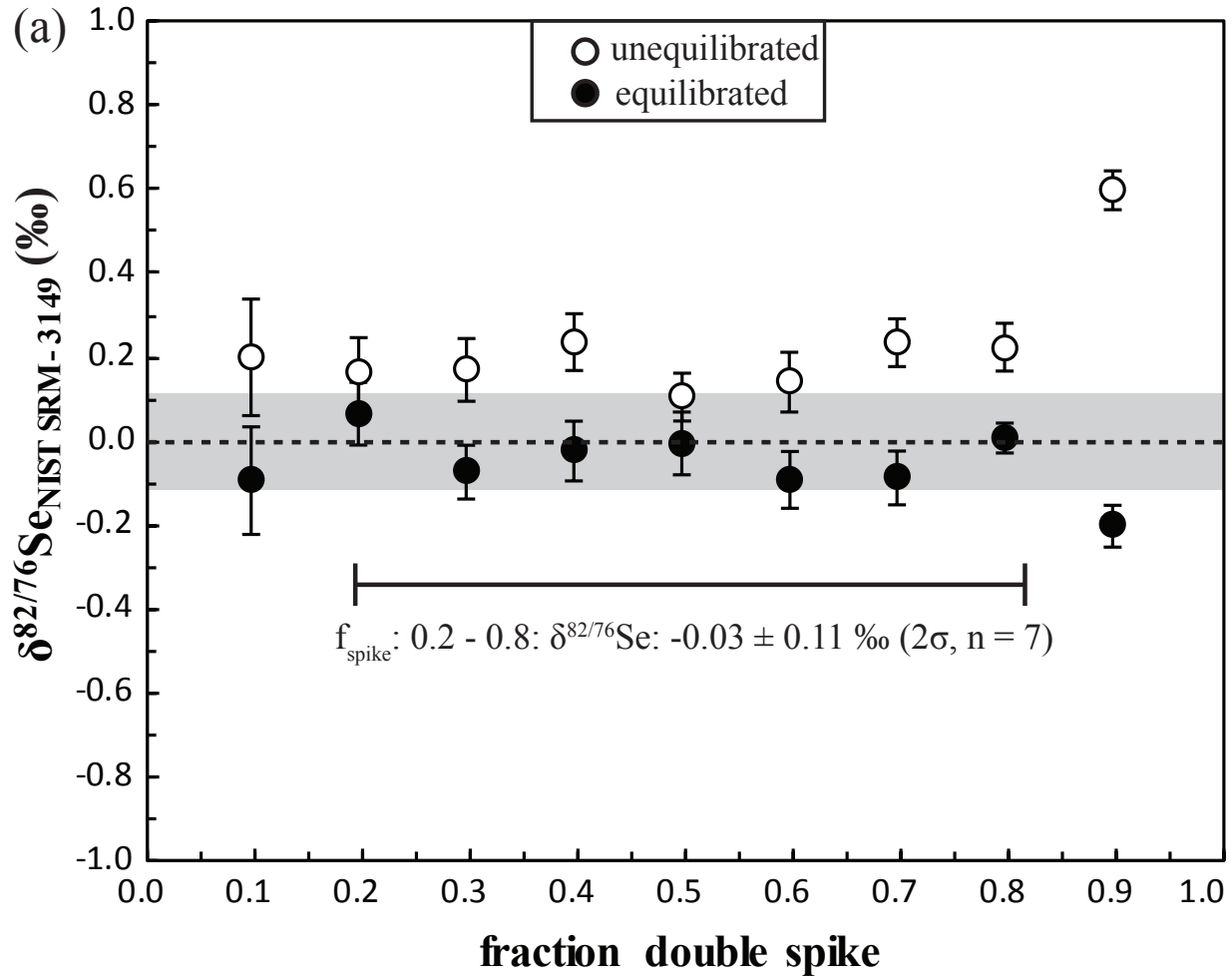
(a)
unequilibrated
equilibrated
$\delta^{82/76}Se_{NIST\ SRM-3149}$ (‰)
f_{spike}: 0.2 - 0.8: $\delta^{82/76}$Se: -0.03 ± 0.11 ‰ (2σ, n = 7)
fraction double spike

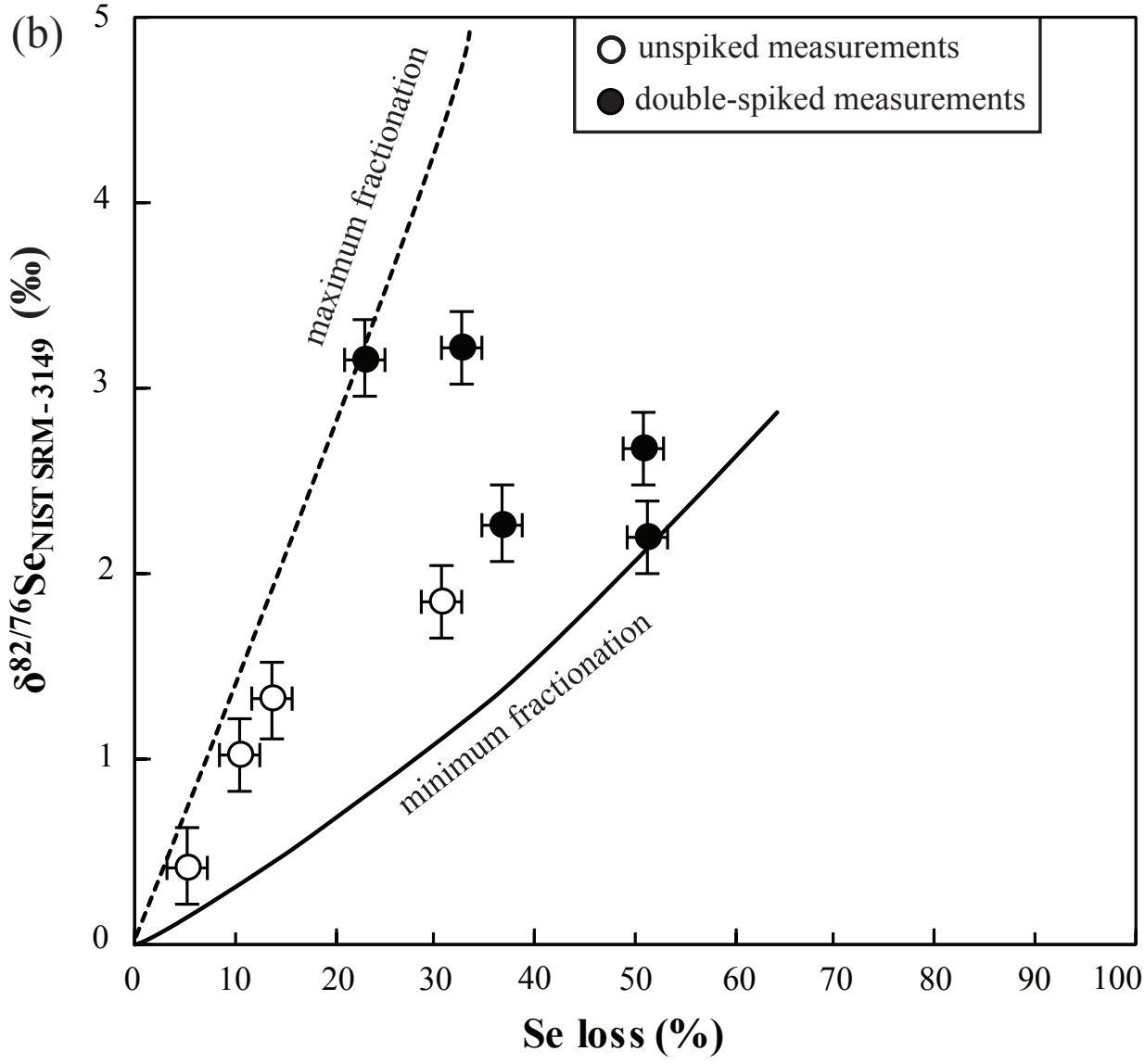
(b)
unspiked measurements
double-spiked measurements
maximum fractionation
minimum fractionation
$\delta^{82/76}Se_{NIST\ SRM-3149}$ (‰)
Se loss (%)

CETAC HGX-200 Hydride Generation and Cold Vapor System

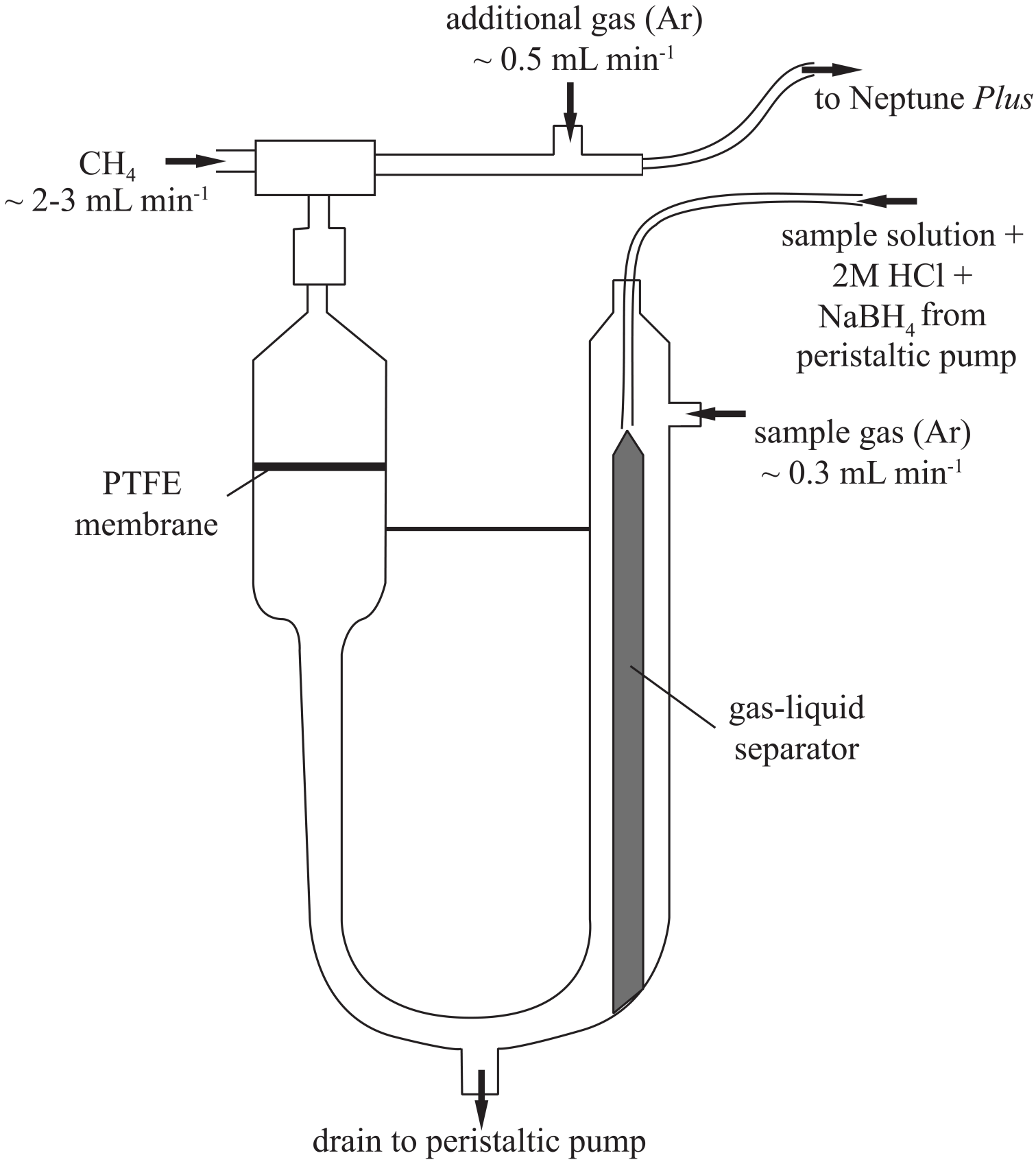

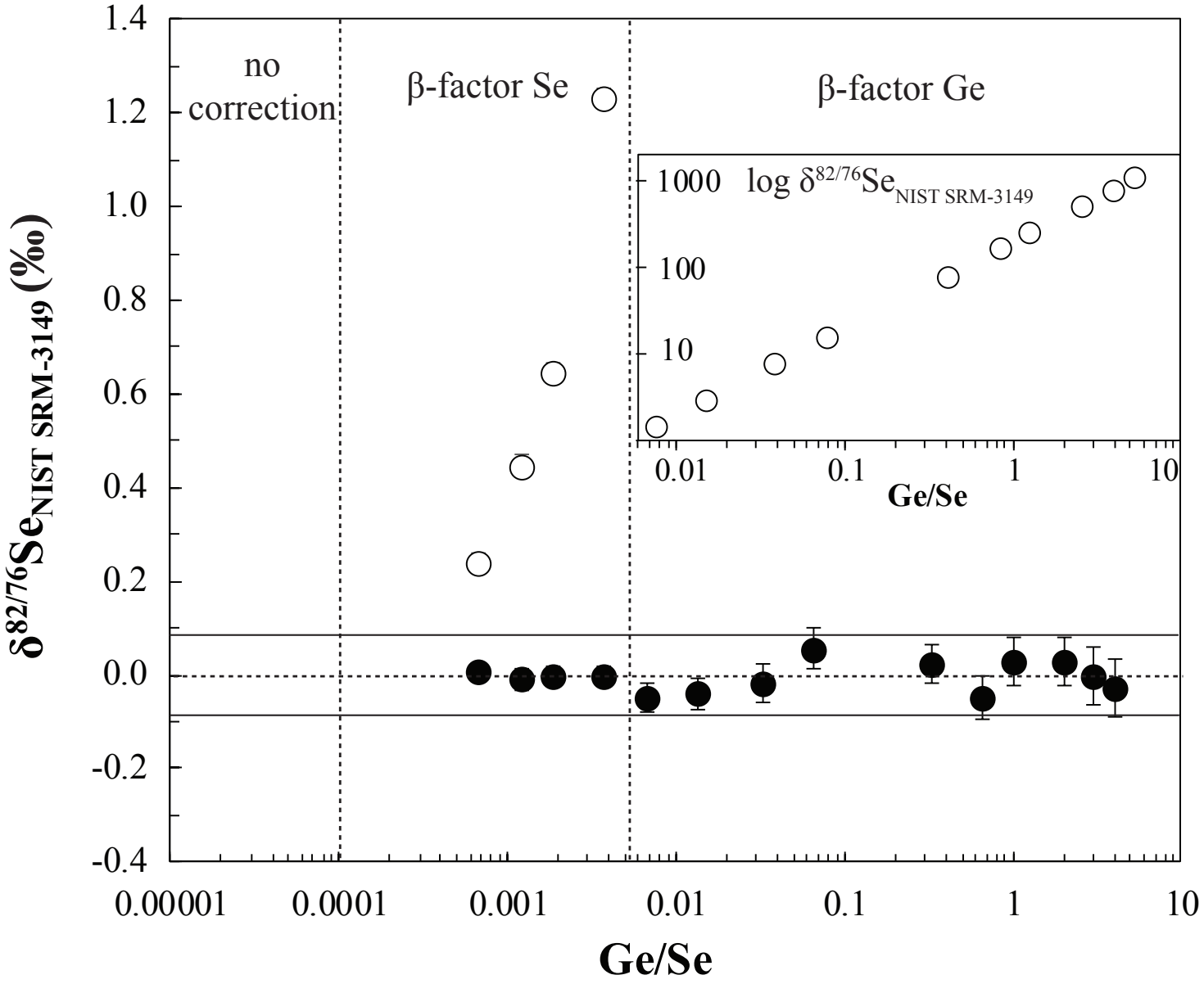
no correction
β-factor Se
β-factor Ge
1000 log δ82/76SeNIST SRM-3149
100
10
0.01
0.1
1
10
Ge/Se
δ82/76SeNIST SRM-3149 (‰)
1.4
1.2
1.0
0.8
0.6
0.4
0.2
0.0
-0.2
-0.4
0.00001
0.0001
0.001
0.01
0.1
1
10
Ge/Se

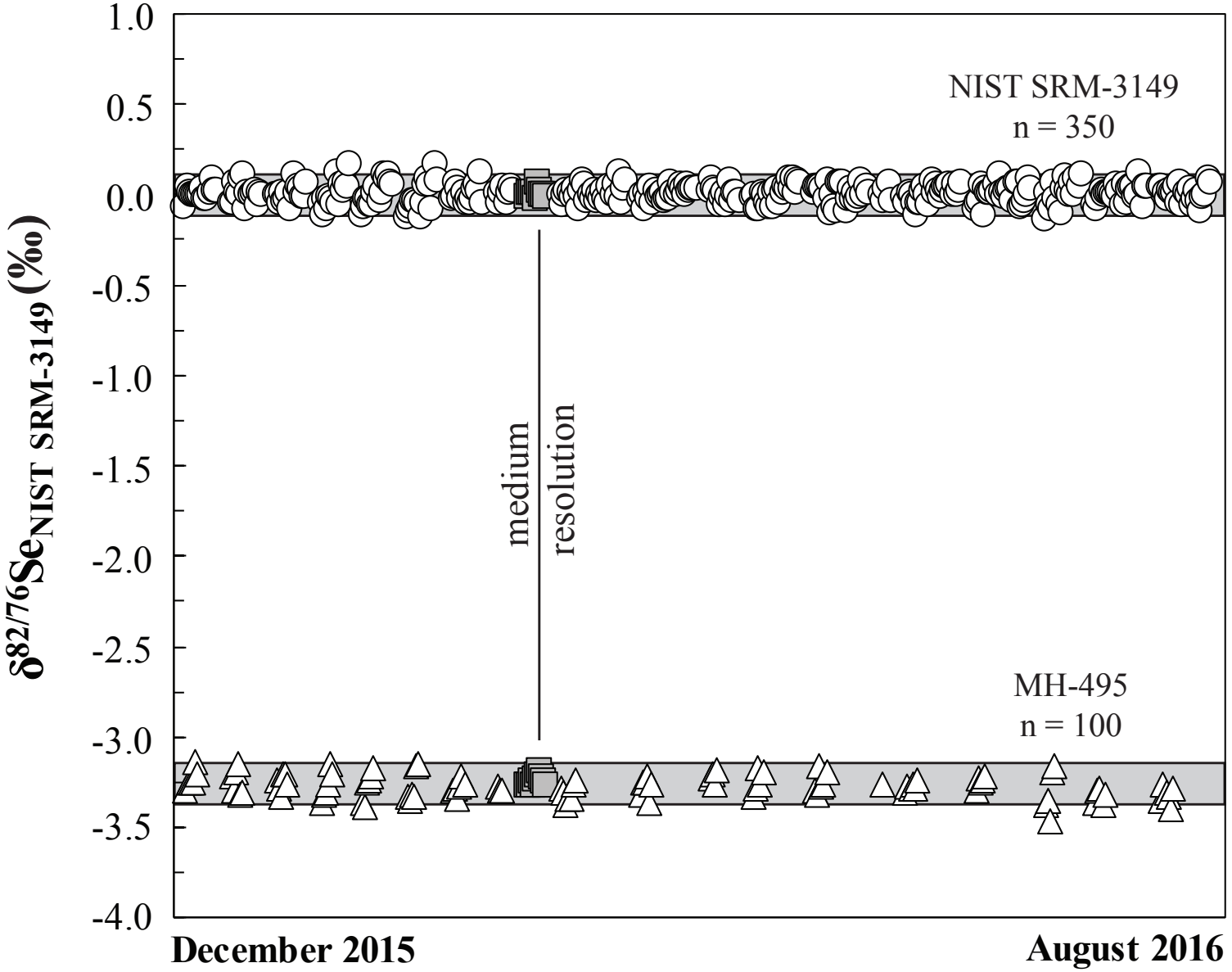
1.0
0.5
0.0
-0.5
-1.0
-1.5
-2.0
-2.5
-3.0
-3.5
-4.0
δ82/76SeNIST SRM-3149 (‰)
NIST SRM-3149
n = 350
medium
resolution
MH-495
n = 100
December 2015
August 2016

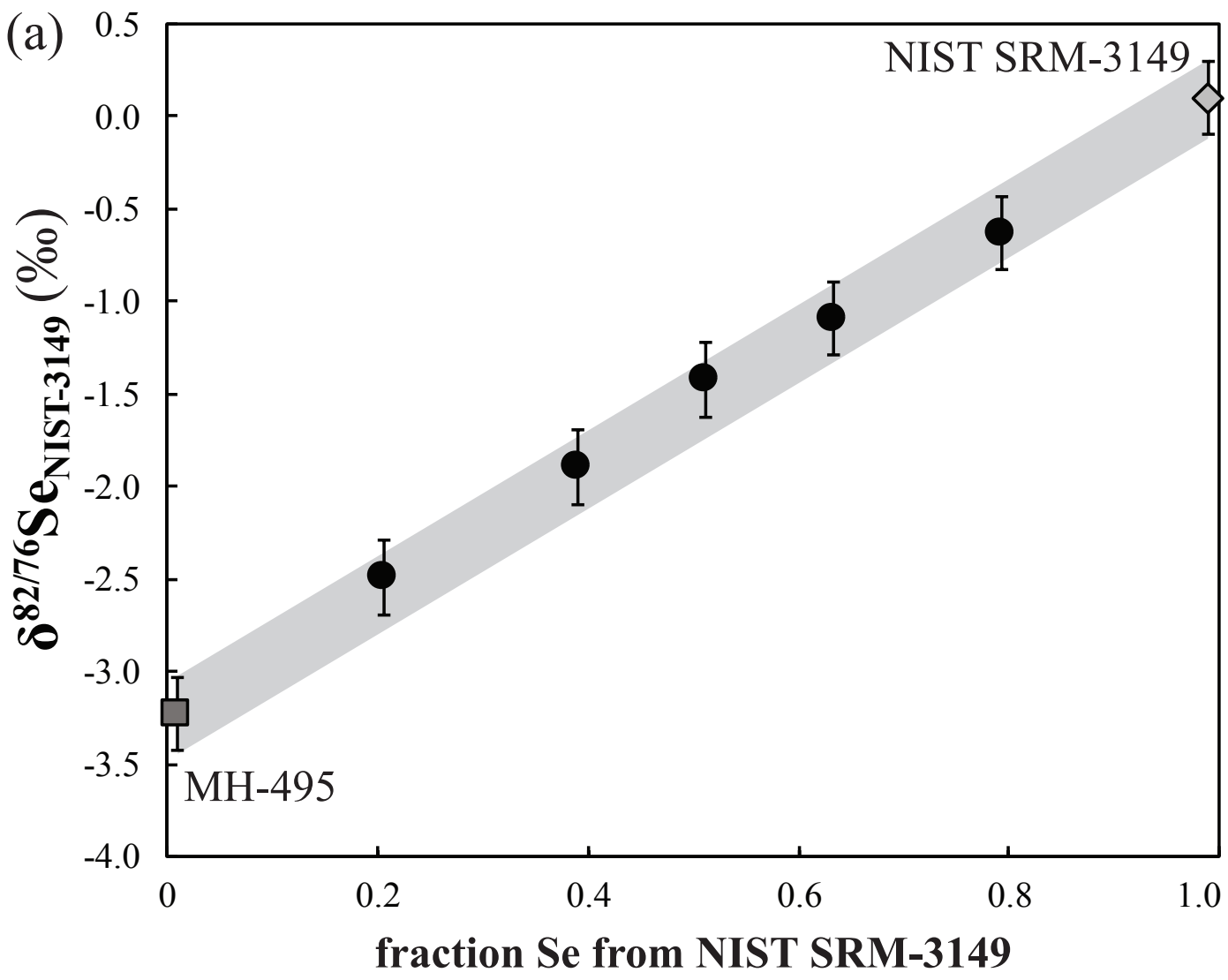
(a)
NIST SRM-3149
MH-495
$\delta^{82/76}Se_{NIST-3149}$ (‰)
fraction Se from NIST SRM-3149
0.5
0.0
-0.5
-1.0
-1.5
-2.0
-2.5
-3.0
-3.5
-4.0
0
0.2
0.4
0.6
0.8
1.0

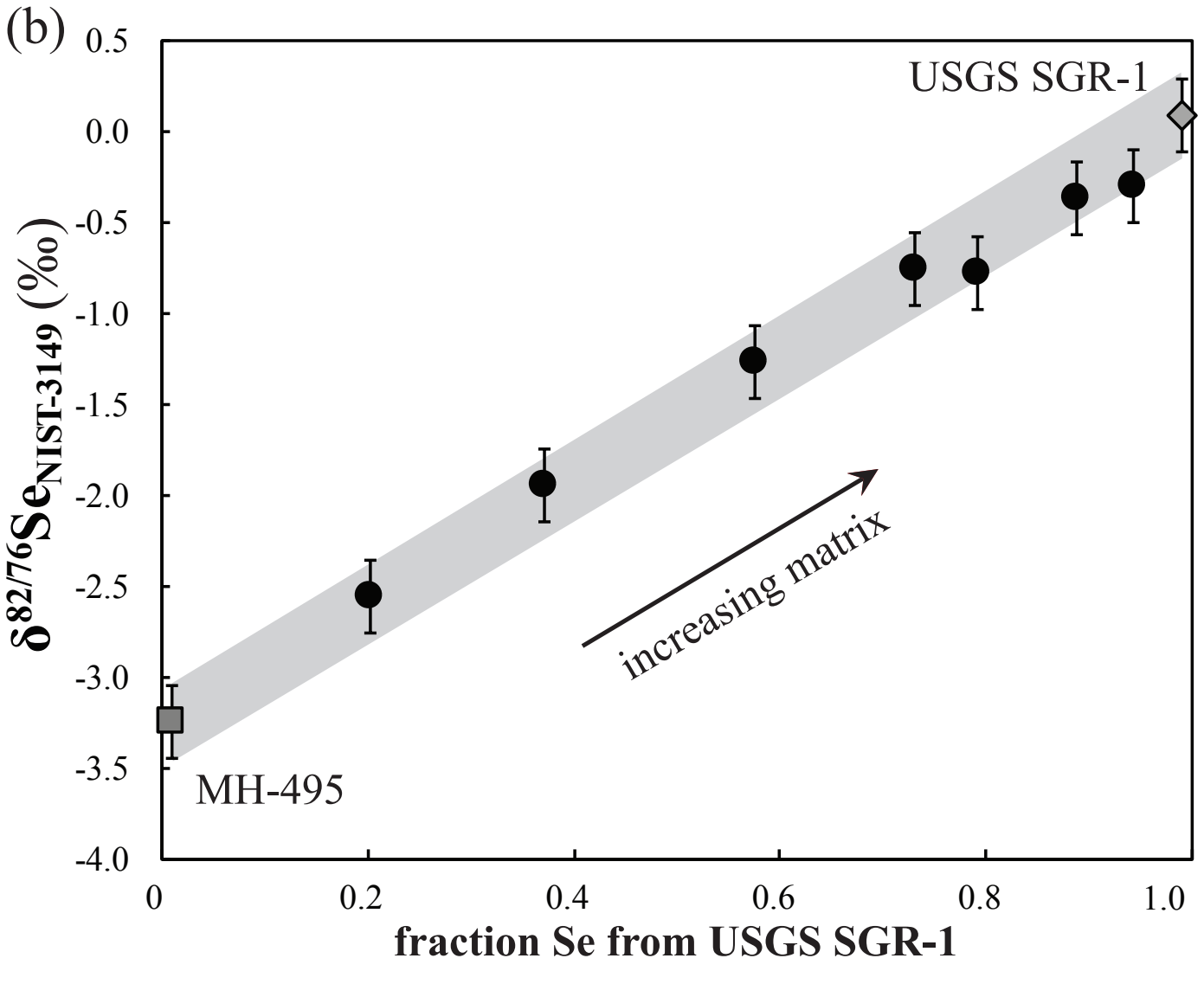
(b)
USGS SGR-1
MH-495
increasing matrix
$\delta^{82/76}Se_{NIST-3149}$ (‰)
fraction Se from USGS SGR-1
0.5
0.0
-0.5
-1.0
-1.5
-2.0
-2.5
-3.0
-3.5
-4.0
0
0.2
0.4
0.6
0.8
1.0

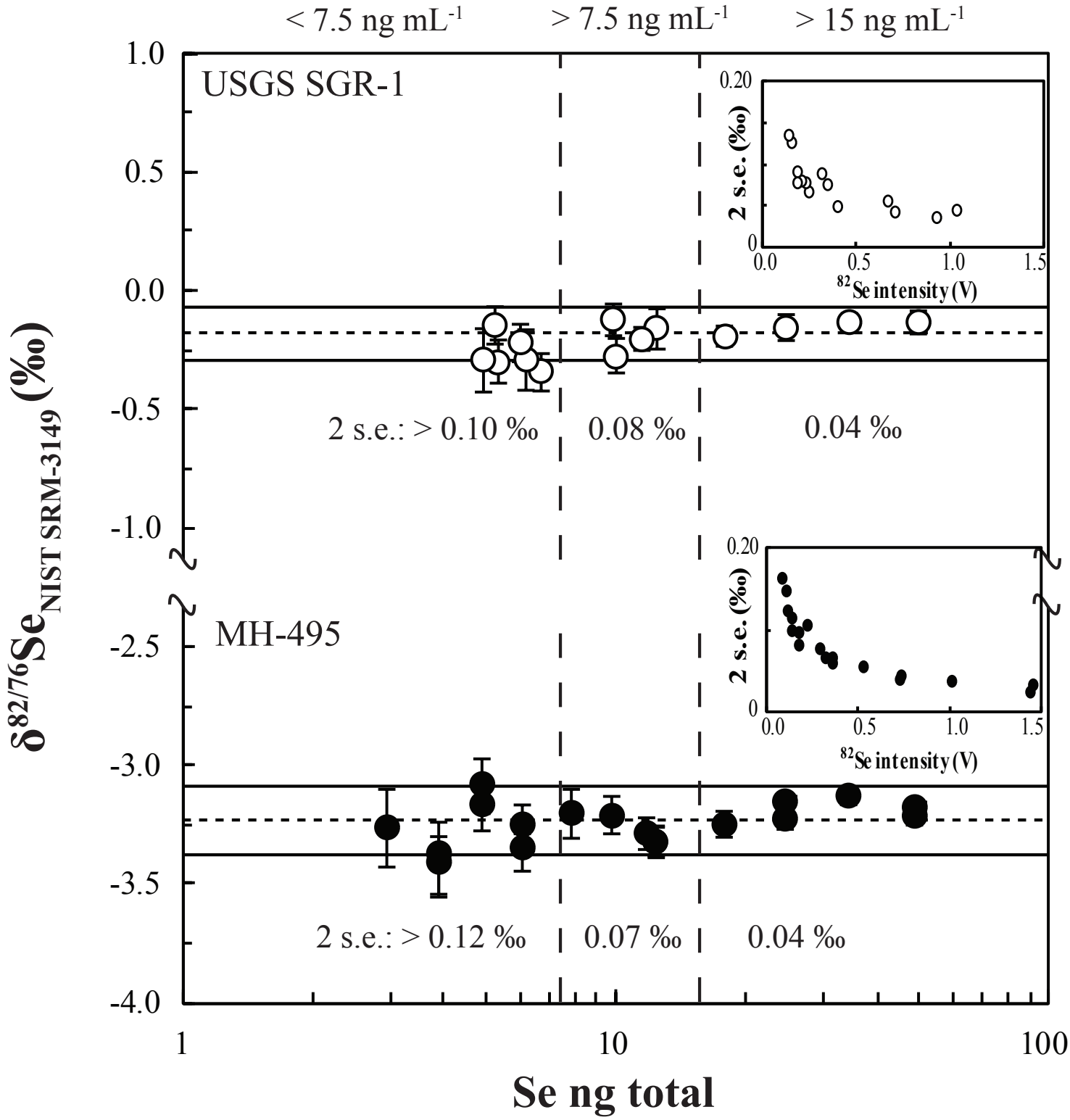
< 7.5 ng mL-1
> 7.5 ng mL-1
> 15 ng mL-1
USGS SGR-1
MH-495
2 s.e.: > 0.10 ‰
0.08 ‰
0.04 ‰
2 s.e.: > 0.12 ‰
0.07 ‰
0.04 ‰
2 s.e. (‰)
82Se intensity (V)
δ82/76SeNIST SRM-3149 (‰)
Se ng total

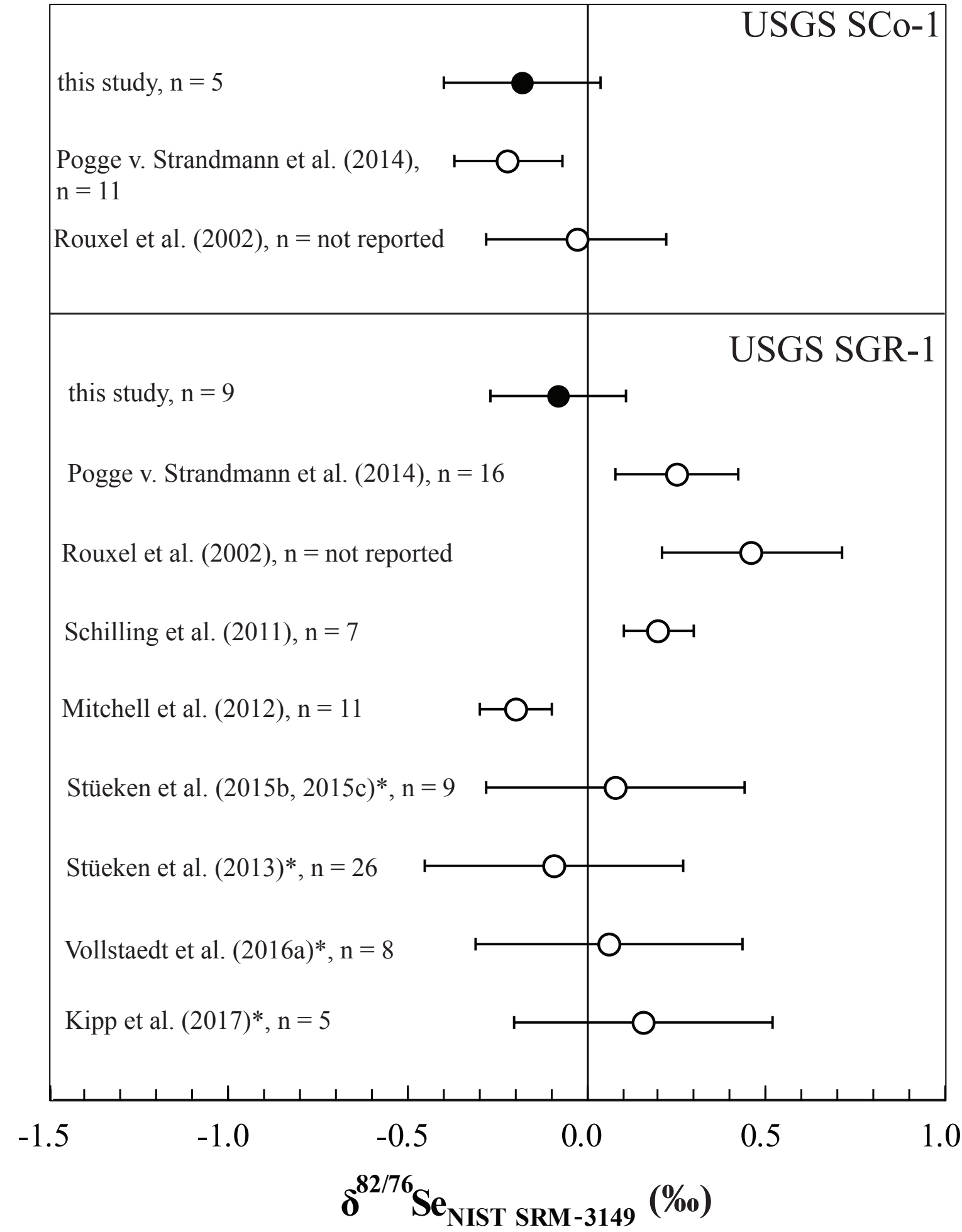
USGS SCo-1
this study, n = 5
Pogge v. Strandmann et al. (2014), n = 11
Rouxel et al. (2002), n = not reported
USGS SGR-1
this study, n = 9
Pogge v. Strandmann et al. (2014), n = 16
Rouxel et al. (2002), n = not reported
Schilling et al. (2011), n = 7
Mitchell et al. (2012), n = 11
Stüeken et al. (2015b, 2015c)*, n = 9
Stüeken et al. (2013)*, n = 26
Vollstaedt et al. (2016a)*, n = 8
Kipp et al. (2017)*, n = 5
-1.5
-1.0
-0.5
0.0
0.5
1.0
δ82/76SeNIST SRM-3149 (‰)

Se masses	74	76	77	78	80	82
Pogge von Strandmann et al. (2014)[1] $^{74\text{-}78\text{-}77\text{-}82}$Se	**45.89%**	-	0.51%	**53.61%**	-	-
Pogge von Strandmann et al. (2014)[1] $^{78\text{-}82\text{-}76\text{-}77}$Se	**-**	0.14%	-	**15.61%**	-	**84.25%**
Vollstaedt et al. (2016a)[2] $^{74\text{-}77\text{-}78\text{-}82}$Se	**62.42%**	-	**37.56%**	0.02%	-	0.00%
Zhu et al. (2008)[3]; Schilling et al. (2011)[3]; Mitchell et al. (2012)[3]	**51.20%**	0.09%	**48.57%**	0.09%	0.03%	0.01%
This study[4] $^{74\text{-}77\text{-}78\text{-}82}$Se	**52.29%**	0.53%	**47.12%**	0.04%	0.02%	0.01%
Rudge et al. (2009) ideal composition for $^{74\text{-}77\text{-}78\text{-}82}$Se	**51.75%**		**48.25%**			

Caption: Table 1: Overview of Se double spike compositions used by different working groups. Bold numbers indicate spike isotopes. Data acquisition at 1: Bristol Isotope Group, School of Earth Sciences, Bristol University, UK. 2: Institute of Geological Sciences, University of Bern, Switzerland. 3: Department of Geology, University of Illinois at Urbana-Champaign, Urbana. 4 (this study): Isotope Geochemistry, University of Tübingen, Germany.

Parameters	
RF power (W)	1200
Acceleration voltage (V)	-10000
Sample cone	Ni Jet
Skimmer cone	Ni H-type
Ar gas flow rates (L min^{-1})	
Coolant	15
Auxiliary	0.7 - 1.0
Sample gas	0.24 - 0.56
Additional gas	0.48 - 0.56
Methane (mL min^{-1})	2.0 - 3.5
Analyte matrix	2 mol L^{-1} HCl
$NaBH_4$	0.4 % (m/m)
Sample uptake (mL min^{-1})	0.235
conc. sample solution (ng mL^{-1})	≤ 15
sample solution volume (mL)	1
Cycle integration time (s)	4.194
Number of cycles per analysis	40
Intensity ^{82}Se (V)	0.5

Caption: Table 2: Operating parameters

Cups	L4	L3	L2			L1	C		H1	H2	H3	H4
Masses	**72**	**73**	**74**	**75**	**76**	**77**	**78**	**79**	**80**	**81**	**82**	**83**
Selenium Abundance (%)			**^{74}Se 0.87**		**^{76}Se 9.36**	**^{77}Se 7.63**	**^{78}Se 23.78**		**^{80}Se 49.61**		**^{82}Se 8.73**	
(i) Plasma induced												
Kr							**^{78}Kr**		**^{80}Kr**		**^{82}Kr**	^{83}Kr
ArAr	^{36}Ar^{36}Ar		**^{38}Ar^{36}Ar**		**^{40}Ar^{36}Ar** **^{38}Ar^{38}Ar**		**^{40}Ar^{38}Ar**		**^{40}Ar^{40}Ar**			
(ii) Plasma and analyte matrix induced												
ArArH		^{36}Ar^{36}ArH		^{38}Ar^{36}ArH		**^{40}Ar^{36}ArH** **^{38}Ar^{38}ArH**		^{40}Ar^{38}ArH		^{40}Ar^{40}ArH		
ArCl		^{38}Ar^{35}Cl ^{36}Ar^{37}Cl		^{40}Ar^{35}Cl ^{38}Ar^{37}Cl		**^{40}Ar^{37}Cl**						
(iii) Analyte and sample matrix induced												
FeO	^{56}Fe^{16}O		**^{58}Fe^{16}O**									
NiO			**^{58}Ni^{16}O**		**^{60}Ni^{16}O**		**^{62}Ni^{16}O**		**^{64}Ni^{16}O**			
ZnO									**^{64}Zn^{16}O**		**^{66}Zn^{16}O**	^{67}Zn^{16}O
Se-H				^{74}SeH		**^{76}SeH**	**^{77}SeH**			^{80}SeH		^{82}SeH
Ge	^{72}Ge	^{73}Ge	**^{74}Ge**		**^{76}Ge**							
Br-H									**^{79}BrH**		**^{81}BrH**	
As-H					**^{75}AsH**							

Caption: Table 3: Measured masses and associated isobaric interferences.

Sample	Sample type	Se (µg g^{-1})	$\delta^{82/76}$Se (‰)	2 s.e (‰)	$\delta^{82/78}$Se (‰)	2 s.e (‰)
USGS SGR-1	Shale	3.70	0.09	0.04	0.06	0.03
		3.63	-0.08	0.05	-0.05	0.03
		3.49	-0.05	0.05	-0.03	0.03
		3.84	-0.18	0.08	-0.12	0.05
		3.95	-0.17	0.07	-0.11	0.05
		4.03	-0.17	0.07	-0.11	0.05
		3.82	0.04	0.06	0.03	0.04
		3.75	-0.13	0.08	-0.08	0.05
		3.66	-0.16	0.07	-0.10	0.05
	medium resolution	3.72	0.03	0.03	0.02	0.02
	AVERAGE	**3.76**	**-0.08**	**0.06**	**-0.05**	**0.04**
	2 s.d.	**0.32**	**0.20**	**0.03**	**0.13**	**0.02**
USGS SCo-1	Shale	0.88	-0.08	0.07	-0.06	0.04
		0.81	-0.34	0.05	-0.22	0.03
		0.85	-0.15	0.07	-0.10	0.04
		0.86	-0.25	0.08	-0.16	0.05
		0.83	-0.09	0.07	-0.06	0.05
	AVERAGE	**0.84**	**-0.18**	**0.07**	**-0.12**	**0.04**
	2 s.d.	**0.06**	**0.22**	**0.02**	**0.14**	**0.01**
USGS BCR-2	Basalt	0.075	0.19	0.06	0.12	0.04
		0.067	0.16	0.05	0.10	0.03
		0.072	0.19	0.06	0.12	0.04
	AVERAGE	**0.071**	**0.18**	**0.06**	**0.12**	**0.04**
	2 s.d.	**0.008**	**0.03**	**0.01**	**0.02**	**0.01**

Caption: Table 4: Se isotope data for USGS reference materials SGR-1, SCo-1 and BCR-2.